

AD-A100 280

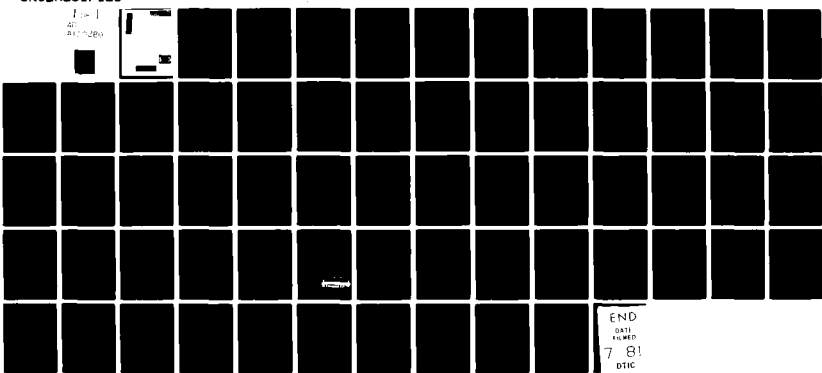
CONTROL DYNAMICS CO HUNTSVILLE AL
ANALYSIS OF SAMPLING RATE ON SAM ACCURACY. (U)
MAY 81 S M SELTZER, H E WORLEY

F/G 16/4.2

DAAH01-81-M-A118
NL

UNCLASSIFIED

100-1
AD-A100
280



END
DATE
RELEASER
1/81
DTIC

LEVEL II
S ①

ADA100280



DISTRIBUTION STATEMENT A
Approved for public release
Distribution Unlimited

Unclassified

SECURITY CLASSIFICATION OF THIS PAGE (When Data Entered)

REPORT DOCUMENTATION PAGE		READ INSTRUCTIONS BEFORE COMPLETING FORM
1. REPORT NUMBER	2. GOVT ACCESSION NO.	3. RECIPIENT'S CATALOG NUMBER
		AD-A100 280
4. TITLE (and Subtitle) Analysis of Sampling Rate on SAM Accuracy	5. TYPE OF REPORT & PERIOD COVERED Final Report 23 Jan 81 - 15 May 81	
7. AUTHOR(s) Sherman M. Seltzer	6. CONTRACT OR GRANT NUMBER(s) DAAH01-81-M-A118 (66)	
9. PERFORMING ORGANIZATION NAME AND ADDRESS Control Dynamics Company 221 East Side Square, Suite 1B Huntsville, AL 35801	10. PROGRAM ELEMENT, PROJECT, TASK AREA & WORK UNIT NUMBERS	
11. CONTROLLING OFFICE NAME AND ADDRESS CMDR, US Army Missile Command MSL Lab Attention: DRSMI-IYE/Glass Redstone Arsenal, AL 35898	12. REPORT DATE 4 May 81	
14. MONITORING AGENCY NAME & ADDRESS (if different from Controlling Office)	13. NUMBER OF PAGES 65	
	15. SECURITY CLASS. (of this report) Unclassified	
	15a. DECLASSIFICATION/DOWNGRADING SCHEDULE	
16. DISTRIBUTION STATEMENT (of this Report) Distribution unlimited; approved for public release		
17. DISTRIBUTION STATEMENT (of the abstract entered in Block 20, if different from Report)		
18. SUPPLEMENTARY NOTES		
19. KEY WORDS (Continue on reverse side if necessary and identify by block number) Guidance Control Anti-Tactical Ballistic Missile (ATBM)		
20. ABSTRACT (Continue on reverse side if necessary and identify by block number) This report covers the efforts undertaken to develop a mathematical model of the FAMMS I surface-to-surface missile suitable for a preliminary analysis of the effects of digital computer sampling on system performance. In particular a methodology for digital autopilot design is developed and exposed by example.		

Accession For	
NTIS GPA&I	<input checked="" type="checkbox"/>
DTIC TAB	<input type="checkbox"/>
Unannounced	<input type="checkbox"/>
Justification	
By _____	
Distribution/ _____	
Availability Codes	
Dist	Available and/or Special
A	

ANALYSIS OF SAMPLING RATE
ON SAM ACCURACY

by

Sherman M. Seltzer
PRINCIPAL INVESTIGATOR

and

H. Eugene Worley
CO-INVESTIGATOR

4 May 1981

FINAL REPORT

This research was performed for the US Army
Missile Command, Redstone Arsenal, Alabama 35898

under

Contract DAAH01-81-M-A118

CONTROL DYNAMICS COMPANY
221 East Side Square, Suite 1B
Huntsville, Alabama 35801

DTIC
SELECTED
S JUN 16 1981 D

DISTRIBUTION STATEMENT A
Approved for public release;
Distribution Unlimited

TABLE OF CONTENTS

LIST OF FIGURES	ii
LIST OF TABLES	iii
ABSTRACT	iv
SECTION I. INTRODUCTION	1
SECTION II. EQUATIONS OF MOTION	3
SECTION III. DIGITAL AUTOPILOT DESIGN	10
SECTION IV. CONCLUSIONS	33
APPENDIX A. DETERMINATION OF DIGITAL CONTROL SYSTEM RESPONSE BY CROSS-MULTIPLICATION	34
APPENDIX B. A VALIDATED METHODOLOGY FOR ACCURATELY PREDICTING MISSILE FLIGHT PERFORMANCE . .	38
REFERENCE	56
DISTRIBUTION LIST	57

LIST OF FIGURES

Fig. 1. PLANAR PORTRAYAL OF FAMMS MISSILE	4
Fig. 2. SYSTEM BLOCK DIAGRAM	11
Fig. 3. PARAMETER PLANE STABILITY BOUNDARY SKETCH . .	20
Fig. 4. PARAMETER PLANE PLOT	21
Fig. 5. PARAMETER PLANE PLOT (ENLARGED SCALE)	23
Fig. 6. UNIT STEP RESPONSE	27
Fig. 7. RAMP RESPONSE	32

LIST OF TABLES

TABLE 1.	SAM EQUATIONS	12
TABLE 2.	CHARACTERISTIC EQUATION COEFFICIENTS . .	14
TABLE 3.	COMPUTER PRINT-OUT FOR PARAMETER PLANE ANALYSIS.	16
TABLE 4.	CLOSED-LOOP TRANSFER FUNCTION NUMERATOR COEFFICIENTS	22
TABLE 5.	COMPUTER PRINT-OUT FOR UNIT STEP RESPONSE	25
TABLE 6.	COMPUTER PRINT-OUT FOR RAMP RESPONSE . .	28

ABSTRACT

This report covers the efforts undertaken to develop a mathematical model of the FAMMS I surface-to-surface missile suitable for preliminary analysis of the effects of digital computer sampling on system performance. Planar equations are developed and linearized to permit digital autopilot design to proceed. A design methodology is developed and described through application to a simplified version of the FAMMS I equations.

SECTION I. INTRODUCTION

The purpose of this work is to establish the technical groundwork for the analysis of the performance of a digital guidance and control (G&C) system for use on an advanced Future Army Modular Missile System (FAMMS). Presently FAMMS is envisioned to be a surface-to-air missile. The tasks described to achieve this analysis are envisioned as:

1. Derive equations of motion;
2. Linearize equations of motion;
3. "Close the loop" by including guidance and control (autopilot);
4. Design and stabilize autopilot;
5. Develop simplified planar time-varying simulation;
6. Develop candidate target models;
7. Design guidance loop(s);
8. Conduct performance studies.

The work reported upon in this document comprises Tasks 1-4 as described below:

1. Derive planar equations of motion;
2. Linearize planar equations of motion;
3. Close the loop with a digital autopilot, assuming a "perfect" guidance command;
4. Design and stabilize a postulated autopilot.

The performance of the postulated autopilot is checked by application of the "Cross-Multiplication" Technique described in Appendix A. It is anticipated that the simulation philosophies

described in Appendix B will be used in part or as a whole for detailed performance studies with the MICOM FAMMS Simulation presently under development.

SECTION II. EQUATIONS OF MOTION

The planar equations of motion of the FAMMS were derived considering the three coordinate systems as depicted in Figure 1. The three coordinate systems are defined as follows:

$\hat{1R}, \hat{3R}$ - Unit vectors defining an inertial coordinate frame used for reference,

$\hat{1b}, \hat{3b}$ - Unit vectors defining a body fixed (missile) coordinate frame,

$\hat{1T}, \hat{3T}$ - Unit vectors defining a target fixed coordinate frame.

The $\hat{1b}, \hat{3b}$ rotates through an angle θ with respect to the $\hat{1R}, \hat{3R}$ inertial reference system. The origin of this body fixed system is defined by the vector R_m , the engine gimbal angle is defined by the angle δ_E , and the aerodynamic surface deflection by the angle δ . The vector equations of motion are then as follows:

$$\ddot{MR_m} = (F-A) \hat{1b} + (F\delta_E - N) \hat{3b} + mg \hat{3R} \quad (\text{II-1})$$

$$\ddot{I\theta} = M - l_0 N - l_E F\delta_E \quad (\text{II-2})$$

Where

F \equiv Engine thrust force

A \equiv Aerodynamic axial force

N \equiv Aerodynamic normal force

M \equiv Aerodynamic pitching moment

l_0 \equiv Distance from vehicle center of mass to moment reference point

l_E \equiv Distance from vehicle center of mass to engine gimbal point.

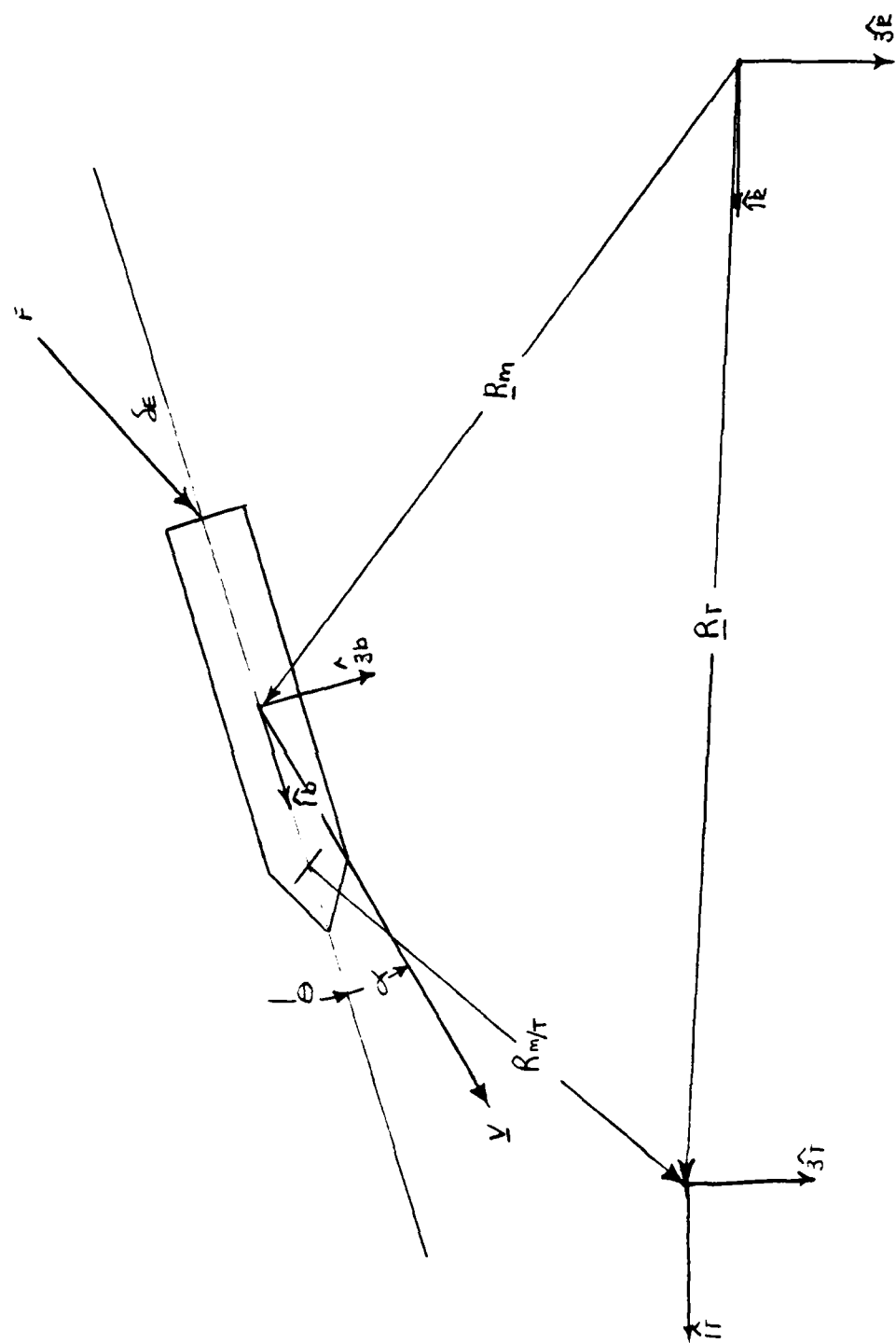


FIGURE 1. Planar Portrayal of FAMMS Missile

Now representing the vector \underline{R}_m as follows:

$$\underline{R}_m = X \hat{1R} + Z \hat{3R},$$

yields the following scalar equations in the inertial coordinate frame

$$\ddot{mX} = (F-A) \cos\theta - (F\delta_E - N) \sin\theta \quad (\text{II-3})$$

$$\ddot{mZ} = (F-A) \sin\theta + (F\delta_E - N) \cos\theta + mg. \quad (\text{II-4})$$

Equations (2), (3), and (4) represent the three nonlinear and time varying differential equations that must be solved to yield the vehicle motion as a function of time. The autopilot and guidance system will provide δ and δ_E as a function of the error conditions.

The equations can then be numerically integrated.

For stability analyses, a linear set of equations is required defined in a body fixed reference system (1b-3b). To derive these linear equations the following definitions are made

$$C_{N\alpha} \equiv \frac{1}{SQ} \left. \frac{\partial N}{\partial \alpha} \right|_{\alpha=0} \quad (\text{II-5})$$

$$C_{m\alpha} \equiv \frac{1}{SQD} \left. \frac{\partial M_0}{\partial \alpha} \right|_{\alpha=0} \quad (\text{II-6})$$

$$C_{A\alpha} \equiv \frac{1}{SQ} \left. \frac{\partial A}{\partial \alpha} \right|_{\alpha=0} \quad (\text{II-7})$$

$$C_{N\delta} \equiv \frac{1}{SQ} \left. \frac{\partial N}{\partial \delta} \right|_{\delta=0} \quad (\text{II-8})$$

$$C_{m\delta} \equiv \frac{1}{SQD} \left. \frac{\partial M}{\partial \delta} \right|_{\delta=0} \quad (II-9)$$

$$C_{A\delta} \equiv \frac{1}{SQ} \left. \frac{\partial A}{\partial \delta} \right|_{\alpha=0} \quad (II-10)$$

$$C_{m\dot{\alpha}} \equiv \frac{1}{SQD} \left. \frac{\partial M}{\partial \dot{\alpha}} \right|_{\alpha=0} \quad (II-11)$$

where

$D \equiv$ Reference vehicle diameter

$$S \equiv \pi D^2 / 4$$

$$Q \equiv (\frac{1}{2}) \rho V^2$$

Thus the linear aerodynamic forces become:

$$N = SQ (C_{N\alpha} \alpha + C_{N\delta} \delta) + N_0 \quad (II-12)$$

$$M = DSQ(C_{m\alpha} \alpha + C_{m\delta} \delta + C_{m\dot{\alpha}} \dot{\alpha}) + M_0 \quad (II-13)$$

$$A = SQ (C_{A\alpha} \alpha + C_{A\delta} \delta) + A_0 \quad (II-14)$$

The left hand side of Equation II-1 can be transformed to a body fixed system through consideration of the following definition

$$\dot{\underline{R}}_m \equiv \hat{U}\hat{1}_b + \hat{W}\hat{3}_b \quad (II-15)$$

where

$U \equiv$ $\hat{1}_b$ component of velocity

$W \equiv$ $\hat{3}_b$ component of velocity.

Thus

$$\ddot{\underline{R}}_m = \dot{\underline{V}} = (\dot{U} + \dot{\theta}W)\hat{1}_b + (\dot{W} - \dot{\theta}U)\hat{3}_b \quad (II-16)$$

Now let

$$U = U_0 + u(t)$$

$$W = w(t)$$

$$\theta = \theta_0 + \theta(t) \quad (II-17)$$

The quantities u , w and θ represent small deviations from the nominal flight condition represented by U_0 and θ_0 . It is also noted that,

$$\alpha = \frac{w}{U_0} . \quad (\text{II-18})$$

Further, define

$$u' \equiv \frac{u}{U_0} . \quad (\text{II-19})$$

The three governing equations of motion can be written as follows considering the vehicle to be initially in static equilibrium.

$$\dot{M}u' = \frac{QS}{U_0} (C_{A\alpha}\alpha + C_{A\delta}\delta) + \frac{mg \cos \theta_0}{U_0} \theta \quad (\text{II-20})$$

$$M\ddot{\alpha} = M\dot{\theta} - \frac{QS}{U_0} (C_{N\alpha}\alpha + C_{N\delta}\delta) - \frac{mg}{U_0} \sin \theta_0 \theta \quad (\text{II-21})$$

$$\begin{aligned} I\ddot{\theta} &= \underline{OSD} (C_{M\alpha}\alpha + C_{M\delta}\delta) - \underline{\ell_0 QS} (C_{N\alpha}\alpha + C_{N\delta}\delta) \\ &\quad + OSD C_{m\alpha}\dot{\alpha} \end{aligned} \quad (\text{II-22})$$

The further assumption is made in these equations in that the only control variable is the aerodynamic fin deflection angle, δ . The design of the autopilot can be facilitated in this study through consideration of Eqs. (II-21) and (II-22) only since there is typically weak coupling with the translational Eq. (II-20). (In aircraft terminology this is the "short period" mode.) If it is further assumed that the missile is in level flight the transfer function between vehicle rate, $\dot{\theta}$, and fin deflection, δ is

$$\frac{\dot{\theta}(s)}{\delta(s)} = \frac{C_{M\delta}' \{s + \tau_{N\alpha} - \tau_{N\delta} (C_{M\alpha}' / C_{M\delta}')\}}{(s^2 + \tau_{N\alpha}s - C_{M\alpha}') \quad (\text{II-23})}$$

$$\text{where } \bar{C}_{N\alpha} \equiv \frac{QS}{MU_0} C_{N\alpha} \quad (\text{II-24})$$

$$\bar{C}_{N\delta} \equiv \frac{QS}{MU_0} C_{N\delta} \quad (\text{II-25})$$

$$\bar{C}_{M\delta} \equiv (C_{M\delta} - \frac{\ell_0}{D} C_{N\delta}) \frac{DOS}{I} \quad (\text{II-26})$$

$$\bar{C}'_{M\alpha} \equiv (C_{M\alpha} - \frac{\ell_\alpha}{D} C_{N\alpha}) \frac{DOS}{I} \quad (\text{II-27})$$

Now for a design example take the following flight conditions

Mach number = 5.0

Altitude = 10,000 meter

θ_0 = 0 degrees

The FAMMS vehicle characteristics at these flight conditions are as follows

$$C_{M\alpha} = -1.7965$$

$$C_{N\alpha} = .064$$

$$C_{M\delta} = -.381$$

$$C_{N\delta} = .002$$

The required values for the transfer function (II-23) are therefore

$$\bar{C}'_{M\delta} = -15.9$$

$$\bar{C}_{N\alpha} = .0006$$

$$\bar{C}_{N\delta} = .0002$$

$$\bar{C}'_{M\alpha} = -65.92$$

Thus (II-23) become

$$\frac{\dot{\theta}(s)}{\delta(s)} = \frac{-15.9(s + .00064)}{(s^2 + .000675s + 65.92)} \quad (\text{II-28})$$

which can be simplified to

$$\frac{\dot{\theta}(s)}{\delta(s)} = \frac{-15.95s}{(s^2 + 65.92)} \equiv \frac{bs}{s^2 + w^2} \quad (\text{II-29})$$

Therefore, transfer function (II-29) is the required pitch-plane transfer function of the FAMMS missile that is required for control system analysis assuming that the guidance system provides a commanded vehicle rate.

SECTION III. DIGITAL AUTOPILOT DESIGN

It is assumed that the task of the digital autopilot is to match the actual angular rate of change of the missile to the commanded rate-of-change. In Section II these variables are denoted $\dot{\theta}$ and $\dot{\theta}_c$, respectively. The autopilot attempts to achieve this goal by developing a commanded aerodynamic vane deflection angle, δ , which is a function of the error between the command angular rate-of-change, $\dot{\theta}_c$, and the sensed angular rate-of-change, $\dot{\theta}$. It is assumed that the sensed variable is exactly equal to the actual variable and that the commanded aerodynamic deflection is exactly equal to the actual deflection. These assumptions can be relaxed in subsequent more detailed design efforts.

In order to cope with expected forms of $\dot{\theta}_c$, a simple digital filter form is used for the autopilot controller, $D(z)$. The system is described in block diagram form on Fig. 2. The following definitions are used:

$$\dot{\varepsilon} = \dot{\theta}_c - \dot{\theta}, \quad (\text{III-1})$$

$$G_{h0}(s) = \frac{1 - e^{-sT}}{s} \text{ ("Zero Order Hold"),} \quad (\text{III-2})$$

and

$$G_p(s) = \frac{\dot{\theta}(s)}{\delta(s)} = \frac{bs}{s^2 + \omega^2} \text{ (developed in Section II).} \quad (\text{III-3})$$

A. Development of Autopilot Equations.

The autopilot equations are developed by applying SAM (Seltzer's Simplified Analytical Method) to the system described in Fig. 1.¹ The six states (x_1, x_2, \dots, x_6) may be assigned by the designer. They are shown in Fig. 2 and defined below in Column 1.

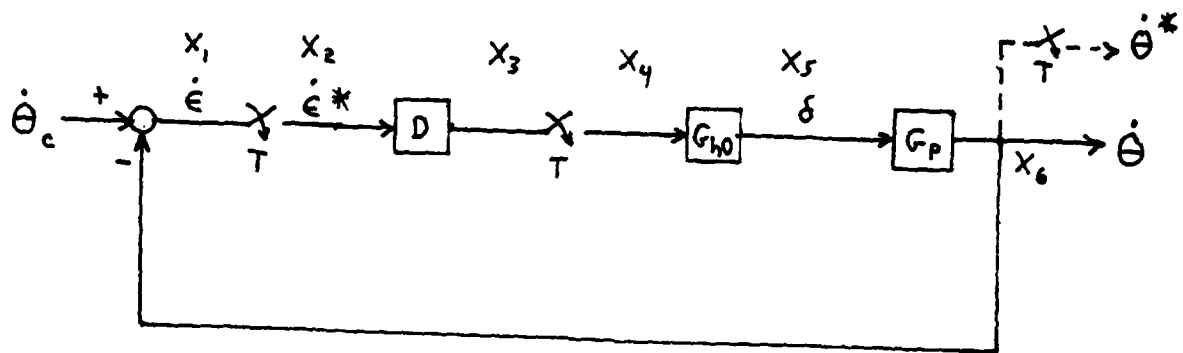


FIGURE 2. System Block Diagram

TABLE I. SAM EQUATIONS

<u>Original Equations</u>	<u>Modified Equations</u>	<u>Pulsed Equations</u>
$x_1 = \dot{\varepsilon} = \dot{\theta}_c - \dot{\theta}$		$x_1^* = \dot{\theta}_c^* - x_6^*$
$x_2 = x_1^*$		$x_2^* = x_1^*$
$x_3 = D x_2$	$x_3 = D x_1^*$	$x_3^* = D^* x_1^*$
$x_4 = x_3^*$		$x_4^* = x_3^*$
$x_5 = G_{h0} x_4$	$x_5 = G_{h0} x_3^*$	$x_5^* = G_{h0}^* x_3^*$
$x_6 = \dot{\theta} = G_p x_5$	$x_6 = G_p G_{h0} x_3^*$	$x_6^* = \dot{\theta}^* = \overline{G_p G_{h0}} * x_3^*$

Applying the rules developed under SAM, state equations x_3 , x_5 , and x_6 must be modified. These modifications are shown in the second column of Table I. The pulsed equations are shown in the third column. As described in Ref. 1, the asterisk is used to symbolize the sampling operation, be it real or analytical. The pulsed concept may be simply described as providing the value of the pulsed variable at each sampling instant T.

B. Development of Closed-Loop Transfer Function.

The pulsed equations developed above may be used to determine the values of the various system variables at (or, with suitable modifications described in Ref. 1, between) sampling instants. However, no indication is easily obtained of system stability or desired performance. One way of obtaining these two important measures is to develop the closed-loop transfer function of the system. This is done by solving x_6^* (which represents $\dot{\theta}^*$) in terms of $\dot{\theta}_c$:

$$x_6^* = \dot{\theta}^* = \overline{G_p G_{h0}}^* x_3^* = \overline{G_p G_{h0}}^* D^* x_1^*$$

$$\begin{aligned}
 x_6^* &= \overline{G_p G_{h0}}^* D^* (\dot{\theta}_c^* - x_6^*) \\
 &= \frac{\overline{G_p G_{h0}}^* D^*}{1 + \overline{G_p G_{h0}}^* D^*} \dot{\theta}_c^*
 \end{aligned} \tag{III-4}$$

Equation (III-4) may be readily transformed into the z-domain to yield the closed-loop transfer function,

$$\frac{\dot{\theta}(z)}{\dot{\theta}_c(z)} = \frac{G_p G_{h0}(z) D(z)}{1 + G_p G_{h0}(z) D(z)}. \tag{III-5}$$

The common definition of z is used, i.e. $z = e^{sT}$, with s being defined as the Laplace operator, $s = \sigma + i\omega = -\zeta\omega_n + \omega_n \sqrt{1 - \zeta^2}$.

Making use of Eqs. (III-2) and (III-3), one may derive the z form $G_p G_{h0}(z)$:

$$\begin{aligned}
 G_p G_{h0}(z) &= \frac{1}{s} \left\{ \frac{(bs)(1 - e^{-sT})}{(s^2 + \omega^2)(s)} \right\} \\
 &= \frac{(b \sin \omega T)(z - 1)}{\omega (z^2 - 2z \cos \omega T + 1)}
 \end{aligned} \tag{III-6}$$

The form of digital filter is the topic of additional study to be performed at a later date. However, the design philosophy may be developed by assuming a ratio of polynomials (in z-domain) for a simple filter that represents the rotational autopilot. That simple form is postulated to be,

$$D(z) = \frac{K_2 z^2 + K_1 z + K_0}{(z - 1)^2} \tag{III-7}$$

Combining Eqs. (III-6) and (III-7), one may obtain

$$F_p G_{h_0}(z) D(z) = \frac{(b \sin \omega T) (K_2 z^2 + K_1 z + K_0)}{\omega (z^2 - 2z \cos \omega T + 1) (z - 1)}. \quad (\text{III-8})$$

One may now substitute Eq. (III-8) into Eq. (III-5) to obtain the system closed-loop transfer function,

$$\frac{\dot{\theta}(z)}{\dot{\theta}_c(z)} = \frac{(b \sin \omega T) (K_2 z^2 + K_1 z + K_0)}{\sum_{j=0}^3 (d_j K_0 + f_j K_1 + g_j)}, \quad (\text{III-9})$$

where the coefficients of the denominator are defined in Table 2.

TABLE 2. CHARACTERISTIC EQUATION COEFFICIENTS

j	d_j	f_j	g_j
0	$b \sin \omega T$	0	$-\omega$
1	0	$b \sin \omega T$	$\omega (1 + 2 \cos \omega T)$
2	0	0	$K_2 b \sin \omega T - \omega (1 + 2 \cos \omega T)$
3	0	0	ω

The denominator of Eq. (III-9), when set equal to zero, constitutes the characteristic equation of the system.

C. Selection of Numerical Values For Autopilot Coefficients

The numerical values of the autopilot coefficients are selected with the use of (of course!) the Parameter Plane technique.² The format of Table 2 was selected to facilitate that use. The numerical values determined in Section II are used for the values

of b and ω (characterizing the operating point about which the open-loop system dynamics were developed). For this example, T is selected as 0.1 sec. and K_2 is selected as 0.01. The Control Dynamics program for using the Parameter Space Technique was used. The output is shown in Table 3 (following pages). The A , B , and F matrices shown at the top of Table 3 are the transposes of the d_j , f_j , and g_j columns of Table 2 when the above-mentioned numerical values for b, ω, K_2 , and T are used.

First, the coordinates for the parameter plane are selected to be K_0 (designated as P_1 in the computer printout) and K_1 (P_2). The stability boundary associated with the singularity at $z = +1$ is found to be (see printout)

$$P_2 = K_1 = -P_1 - 0.01 = -K_0 - 0.01 . \quad (\text{III-10})$$

Similarly, the boundary associated with the singularity at $z = -1$ is found to be

$$P_2 = K_1 = P_1 + 4.7599 = K_0 + 4.7599. \quad (\text{III-11})$$

The boundary associated with the unit circle, $z = e^{i\omega_n T}$, is printed in Table 3 as a function of the argument, $\omega_n T$. Opposite each incremented value of $\omega_n T$ is printed the Jacobian and the associated values of P_1 and P_2 . Since the Jacobian (J) does not change sign, there is no value of $\omega_n T$ where a boundary associated with $J=0$ occurs. The three boundaries are sketched on Fig. 3 and plotted on Fig. 4. Finally, a ζ -contour of $\zeta = 0.5$ is determined and plotted on Figures 4 and 5. The scale of the region of stability

TABLE 3. COMPUTER PRINT-OUT FOR PARAMETER PLANE ANALYSIS

Z TRANSFORM METHOD
THE SYSTEM ORDER IS = 3

ELEMENTS OF A MATRIX A(0),A(1),A(2),...
-1.1542E+01 0.0000E+00 0.0000E+00 0.0000E+00

ELEMENTS OF B MATRIX B(0),B(1),B(2),...
0.0000E+00 -1.1542E+01 0.0000E+00 0.0000E+00

ELEMENTS OF F MATRIX F(0),F(1),F(2),...
-8.1189E+00 1.9293E+01 -1.9408E+01 8.1189E+00

ZETA = 0.0000E+00
THE STABILITY BOUNDARIES FOR Z=+1 AND -1 ARE AS FOLLOWS

FOR Z=-1
P2= 1.0000E+00 *P1 + 4.7599E+00

THE AXES INTERCEPTS ARE AS FOLLOWS:
AT P1=0 , P2= 4.7599E+00
AND AT P2=0 , P1=-4.7599E+00

FOR Z=+1
P2=-1.0000E+00 *P1 + -1.0000E-02

THE AXES INTERCEPTS ARE AS FOLLOWS:
AT P1=0 , P2=-1.0000E-02
AND AT P2=0 , P1=-1.0000E-02

INITIAL OMEGA = 0.0000E+00	FINAL OMEGA = 3.1416E+00		
NUMBER OF STEPS= 50			
WnT= 1.0000E-25	DET= 1.3321E-23	P1=-4.2876E-01	P2= 4.1876E-01
WnT= 6.2832E-02	DET= 8.3645E+00	P1=-4.2598E-01	P2= 4.1430E-01
WnT= 1.2566E-01	DET= 1.6696E+01	P1=-4.1767E-01	P2= 4.0108E-01
WnT= 1.8850E-01	DET= 2.4962E+01	P1=-4.0284E-01	P2= 3.7953E-01
WnT= 2.5133E-01	DET= 3.3129E+01	P1=-3.8456E-01	P2= 3.5040E-01
WnT= 3.1416E-01	DET= 4.1165E+01	P1=-3.5990E-01	P2= 3.1467E-01
WnT= 3.7699E-01	DET= 4.9039E+01	P1=-3.1996E-01	P2= 2.7362E-01
WnT= 4.3982E-01	DET= 5.6720E+01	P1=-2.9486E-01	P2= 2.3874E-01
WnT= 5.0265E-01	DET= 6.4176E+01	P1=-2.6474E-01	P2= 1.6172E-01
WnT= 5.6548E-01	DET= 7.1379E+01	P1=-2.0275E-01	P2= 1.1445E-01
WnT= 6.2832E-01	DET= 7.8391E+01	P1=-1.2007E-01	P2= 8.3930E-02
WnT= 6.9115E-01	DET= 8.4914E+01	P1=-1.0590E-01	P2= 4.7296E-02

WnT= 7.5398E-01	DET= 9.1191E+01	P1=-4.7455E-02	P2= 1.1731E-02
WnT= 8.1681E-01	DET= 9.7108E+01	P1= 1.5040E-02	P2=-1.5551E-02
WnT= 8.7965E-01	DET= 1.0264E+02	P1= 8.1336E-02	P2=-3.2355E-02
WnT= 9.4248E-01	DET= 1.0777E+02	P1= 1.5117E-01	P2=-3.6541E-02
WnT= 1.0053E+00	DET= 1.1248E+02	P1= 2.2427E-01	P2=-2.6070E-02
WnT= 1.0681E+00	DET= 1.1674E+02	P1= 3.0034E-01	P2= 9.6031E-04
WnT= 1.1310E+00	DET= 1.2054E+02	P1= 3.7909E-01	P2= 4.6273E-02
WnT= 1.1938E+00	DET= 1.2386E+02	P1= 4.6020E-01	P2= 1.1138E-01
WnT= 1.2566E+00	DET= 1.2669E+02	P1= 5.4336E-01	P2= 1.9754E-01
WnT= 1.3195E+00	DET= 1.2903E+02	P1= 6.2823E-01	P2= 3.0576E-01
WnT= 1.3823E+00	DET= 1.3085E+02	P1= 7.1448E-01	P2= 4.3672E-01
WnT= 1.4451E+00	DET= 1.3216E+02	P1= 8.0178E-01	P2= 5.9080E-01
WnT= 1.5080E+00	DET= 1.3295E+02	P1= 8.8977E-01	P2= 7.6803E-01
WnT= 1.5708E+00	DET= 1.3321E+02	P1= 9.7810E-01	P2= 9.6810E-01
WnT= 1.6336E+00	DET= 1.3295E+02	P1= 1.0664E+00	P2= 1.1904E+00
WnT= 1.6965E+00	DET= 1.3216E+02	P1= 1.1544E+00	P2= 1.4338E+00
WnT= 1.7593E+00	DET= 1.3085E+02	P1= 1.2417E+00	P2= 1.6971E+00
WnT= 1.8221E+00	DET= 1.2903E+02	P1= 1.3280E+00	P2= 1.9785E+00
WnT= 1.8850E+00	DET= 1.2669E+02	P1= 1.4128E+00	P2= 2.2760E+00
WnT= 1.9478E+00	DET= 1.2386E+02	P1= 1.4860E+00	P2= 2.5874E+00
WnT= 2.0106E+00	DET= 1.2054E+02	P1= 1.5771E+00	P2= 2.9101E+00
WnT= 2.0735E+00	DET= 1.1674E+02	P1= 1.6559E+00	P2= 3.2413E+00
WnT= 2.1363E+00	DET= 1.1248E+02	P1= 1.7319E+00	P2= 3.5780E+00
WnT= 2.1991E+00	DET= 1.0777E+02	P1= 1.8050E+00	P2= 3.9170E+00
WnT= 2.2619E+00	DET= 1.0264E+02	P1= 1.8749E+00	P2= 4.2551E+00
WnT= 2.3248E+00	DET= 9.7108E+01	P1= 1.9412E+00	P2= 4.5868E+00
WnT= 2.3876E+00	DET= 9.1191E+01	P1= 2.0037E+00	P2= 4.9149E+00
WnT= 2.4504E+00	DET= 8.4914E+01	P1= 2.0621E+00	P2= 5.2239E+00
WnT= 2.5133E+00	DET= 7.8301E+01	P1= 2.1163E+00	P2= 5.5305E+00
WnT= 2.5761E+00	DET= 7.1379E+01	P1= 2.1660E+00	P2= 5.8135E+00
WnT= 2.6389E+00	DET= 6.4176E+01	P1= 2.2109E+00	P2= 6.0759E+00
WnT= 2.7018E+00	DET= 5.6720E+01	P1= 2.2511E+00	P2= 6.3147E+00
WnT= 2.7646E+00	DET= 4.9039E+01	P1= 2.2862E+00	P2= 6.5274E+00
WnT= 2.8274E+00	DET= 4.1165E+01	P1= 2.3161E+00	P2= 6.7116E+00
WnT= 2.8903E+00	DET= 3.3129E+01	P1= 2.3406E+00	P2= 6.8652E+00
WnT= 2.9531E+00	DET= 2.4962E+01	P1= 2.3600E+00	P2= 6.9865E+00
WnT= 3.0159E+00	DET= 1.6696E+01	P1= 2.3739E+00	P2= 7.0742E+00
WnT= 3.0788E+00	DET= 8.3645E+00	P1= 2.3822E+00	P2= 7.1272E+00
WnT= 3.1416E+00	DET= 1.3321E-07	P1= 2.3850E+00	P2= 7.1449E+00

ZETA = 5.0000E-01

INITIAL OMEGA = 0.0000E+00

FINAL OMEGA = 3.1416E+00

NUMBER OF STEPS= 50

WnT= 1.0000E-25	DET= 1.1537E-23	P1=-4.2876E-01	P2= 4.1876E-01
WnT= 6.2832E-02	DET= 7.0210E+00	P1=-4.9273E-01	P2= 3.9126E-01
WnT= 1.2566E-01	DET= 1.3588E+01	P1=-3.7874E-01	P2= 3.6377E-01
WnT= 1.8850E-01	DET= 1.9702E+01	P1=-3.5705E-01	P2= 2.3764E-01
WnT= 2.5133E-01	DET= 2.5369E+01	P1=-3.3782E-01	P2= 3.1485E-01
WnT= 3.1416E-01	DET= 3.0594E+01	P1=-3.2113E-01	P2= 2.9601E-01
WnT= 3.7699E-01	DET= 3.5384E+01	P1=-3.0703E-01	P2= 2.8234E-01
WnT= 4.3982E-01	DET= 3.9746E+01	P1=-2.9547E-01	P2= 2.7488E-01
WnT= 5.0265E-01	DET= 4.3691E+01	P1=-2.8642E-01	P2= 2.7368E-01
WnT= 5.6549E-01	DET= 4.7229E+01	P1=-2.7976E-01	P2= 2.7993E-01
WnT= 6.2832E-01	DET= 5.0370E+01	P1=-2.7539E-01	P2= 2.9144E-01
WnT= 6.9115E-01	DET= 5.3129E+01	P1=-2.7314E-01	P2= 3.1466E-01
WnT= 7.5398E-01	DET= 5.5514E+01	P1=-2.7291E-01	P2= 3.4351E-01
WnT= 8.1681E-01	DET= 5.7543E+01	P1=-2.7452E-01	P2= 3.7984E-01
WnT= 8.7965E-01	DET= 5.9226E+01	P1=-2.7730E-01	P2= 4.1394E-01
WnT= 9.4248E-01	DET= 6.0583E+01	P1=-2.8261E-01	P2= 4.7296E-01
WnT= 1.0053E+00	DET= 6.1635E+01	P1=-2.8777E-01	P2= 5.3075E-01
WnT= 1.0681E+00	DET= 6.2267E+01	P1=-2.9614E-01	P2= 5.9353E-01
WnT= 1.1310E+00	DET= 6.2826E+01	P1=-3.0455E-01	P2= 6.6166E-01

WnT= 1.1938E+00	DET= 6.3016E+01	P1=-3.1388E-01	P2= 7.3445E-01
WnT= 1.2566E+00	DET= 6.2954E+01	P1=-3.2397E-01	P2= 8.1124E-01
WnT= 1.3195E+00	DET= 6.2655E+01	P1=-3.3470E-01	P2= 8.9134E-01
WnT= 1.3823E+00	DET= 6.2134E+01	P1=-3.4595E-01	P2= 9.7402E-01
WnT= 1.4451E+00	DET= 6.1407E+01	P1=-3.5760E-01	P2= 1.0586E+00
WnT= 1.5080E+00	DET= 6.0490E+01	P1=-3.6956E-01	P2= 1.1443E+00
WnT= 1.5708E+00	DET= 5.9397E+01	P1=-3.8173E-01	P2= 1.2305E+00
WnT= 1.6336E+00	DET= 5.8144E+01	P1=-3.9402E-01	P2= 1.3166E+00
WnT= 1.6965E+00	DET= 5.6744E+01	P1=-4.0636E-01	P2= 1.4018E+00
WnT= 1.7593E+00	DET= 5.5213E+01	P1=-4.1867E-01	P2= 1.4857E+00
WnT= 1.8221E+00	DET= 5.3563E+01	P1=-4.3090E-01	P2= 1.5676E+00
WnT= 1.8850E+00	DET= 5.1810E+01	P1=-4.4299E-01	P2= 1.6471E+00
WnT= 1.9478E+00	DET= 4.9964E+01	P1=-4.5489E-01	P2= 1.7236E+00
WnT= 2.0106E+00	DET= 4.8041E+01	P1=-4.6657E-01	P2= 1.7969E+00
WnT= 2.0735E+00	DET= 4.6050E+01	P1=-4.7799E-01	P2= 1.8666E+00
WnT= 2.1363E+00	DET= 4.4005E+01	P1=-4.8912E-01	P2= 1.9323E+00
WnT= 2.1991E+00	DET= 4.1915E+01	P1=-4.9993E-01	P2= 1.9938E+00
WnT= 2.2619E+00	DET= 3.9793E+01	P1=-5.1041E-01	P2= 2.0510E+00
WnT= 2.3248E+00	DET= 3.7648E+01	P1=-5.2054E-01	P2= 2.1036E+00
WnT= 2.3876E+00	DET= 3.5489E+01	P1=-5.3031E-01	P2= 2.1515E+00
WnT= 2.4504E+00	DET= 3.3326E+01	P1=-5.3973E-01	P2= 2.1949E+00
WnT= 2.5133E+00	DET= 3.1168E+01	P1=-5.4876E-01	P2= 2.2334E+00
WnT= 2.5761E+00	DET= 2.9021E+01	P1=-5.5742E-01	P2= 2.2674E+00
WnT= 2.6389E+00	DET= 2.6895E+01	P1=-5.6570E-01	P2= 2.2966E+00
WnT= 2.7018E+00	DET= 2.4795E+01	P1=-5.7362E-01	P2= 2.3214E+00
WnT= 2.7646E+00	DET= 2.2727E+01	P1=-5.8118E-01	P2= 2.3417E+00
WnT= 2.8274E+00	DET= 2.0699E+01	P1=-5.8837E-01	P2= 2.3578E+00
WnT= 2.8903E+00	DET= 1.8716E+01	P1=-5.9521E-01	P2= 2.3698E+00
WnT= 2.9531E+00	DET= 1.6731E+01	P1=-6.0171E-01	P2= 2.3778E+00
WnT= 3.0159E+00	DET= 1.4900E+01	P1=-6.0787E-01	P2= 2.3822E+00
WnT= 3.0788E+00	DET= 1.3077E+01	P1=-6.1371E-01	P2= 2.3830E+00
WnT= 3.1416E+00	DET= 1.1314E+01	P1=-6.1923E-01	P2= 2.3805E+00

COEFFICIENTS OF THE CHARACTERISTIC EQUATION WITH

P1=-2.8770E-01 P2= 5.3075E-01

C(0) + C(1)*S + C(2)*S^2 + C(3)*S^3 + ...
C(0)=-4.798301E+00
C(1)= 1.316675E+01
C(2)=-1.940799E+01
C(3)= 8.118882E+00

ROOTS:

REAL	IMAGINARY	DAMPING RATIO	WnT
1.811799E+00	-1.231697E-12	-1.000000E+00	4.773506E-01
3.893382E-01	-4.637780E-01	4.384645E-01	1.006372E+00
3.893382E-01	4.637780E-01	4.384645E-01	1.006372E+00

COEFFICIENTS OF THE CHARACTERISTIC EQUATION WITH
P1=-3.2113E-01 P2= 2.9600E-01

C(0) + C(1)*S + C(2)*S^2 + C(3)*S^3 + ...
C(0)=-4.412458E+00
C(1)= 1.587619E+01
C(2)=-1.940799E+01
C(3)= 8.118882E+00

ROOTS:

REAL	IMAGINARY	DAMPING RATIO	WnT
8.232520E-01	-2.297163E-01	4.997583E-01	3.141594E-01
7.439712E-01	3.031605E-12	1.000000E+00	2.957530E-01
8.232520E-01	2.297163E-01	4.997583E-01	3.141594E-01

You have selected to print data from the parameter plane program.
This program placed on the tape the values of P2 as a function of
P1. You will be given the maximum and minimum values of these variables
but you can select any value you wish for plotting purposes.
P1 is equivalent to X and P2 is equivalent to Y.

CASE #	MIN X	MAX X	MIN Y	MAX Y
1	-4.29E-01	2.38E+00	-3.65E-02	7.14E+00
2	-6.19E-01	-2.73E-01	2.74E-01	2.38E+00

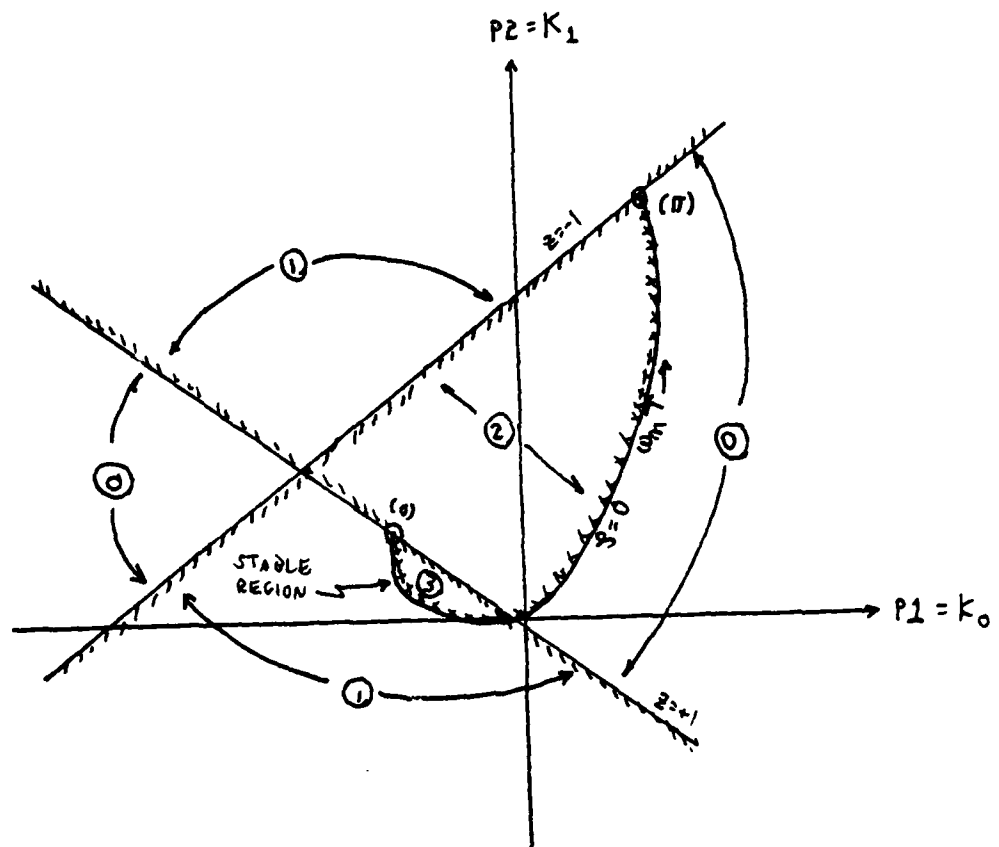


FIGURE 3 Parameter Plane Stability Boundary Sketch

NOTE: Single cross-hatched lines are $z = +1$ and $z = -1$ boundaries.

Double cross-hatched curve is $\zeta = 0$ boundary.

Encircled number represent number of stable roots
in indicated region.

XMIN = -1.000E+00 XMAX = 2.500E+00
YMIN = -1.000E-01 YMAX = 7.500E+00
X tic marks at every 5.000E-01
Y tic marks at every 1.000E+00

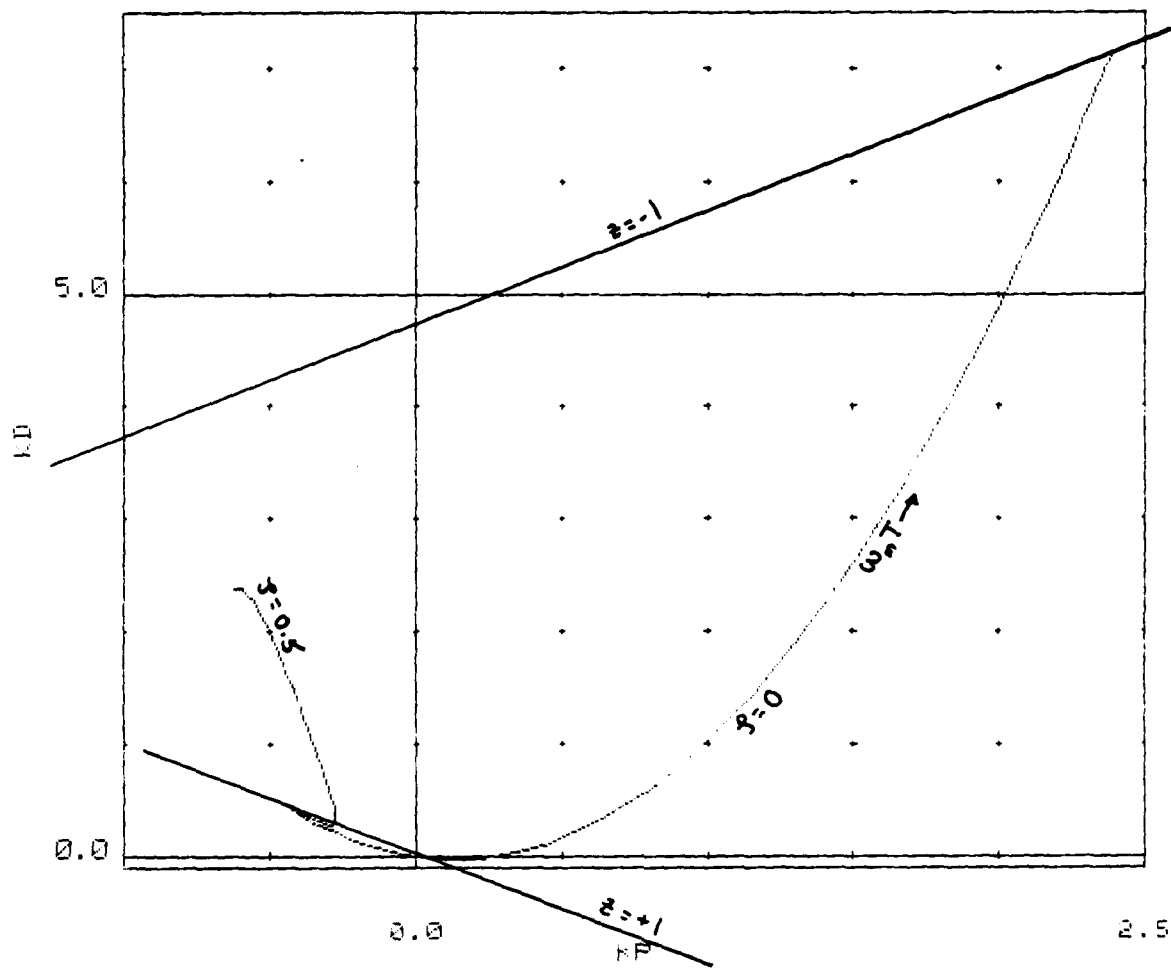


FIGURE 4 Parameter Plane Plot

is increased and shown in Fig. 5 to facilitate selection of a robust design point. That point (underlined in the printout) is

$$P_1 = K_0 = -0.32113$$

and

$$P_2 = K_1 = 0.29601.$$

D. Performance of System

The performance of the candidate design is evaluated by applying the Cross-Multiplication Technique (Appendix A) to the closed-loop transfer function of Eq. (III-9). The coefficients of Eq. (III-9) are re-named and re-cast as

$$\frac{\dot{\theta}(z)}{\dot{\theta}_c(z)} = \frac{\sum_{j=0}^2 n_j z^j}{\sum_{j=0}^3 h_j z^j}. \quad (\text{III-12})$$

where

$$h_j = d_j K_0 + f_j K_1 + g_j \quad (\text{III-13})$$

and the numerator coefficients are defined in Table 4.

TABLE 4. NUMERATOR COEFFICIENTS

j	n _j
0	K ₀ b sin ωT
1	K ₁ b sin ωT
2	K ₂ b sin ωT

You have selected to print data from the parameter plane program. This program placed on the tape the values of P2 as a function of P1. You will be given the maximum and minimum values of these variables but you can select any value you wish for plotting purposes. P1 is equivalent to X and P2 is equivalent to Y.

CASE #	MIN X	MAX X	MIN Y	MAX Y
1	-4.29E-01	2.38E+00	-3.65E-02	7.14E+00
2	-6.19E-01	-2.73E-01	2.74E-01	2.38E+00
	XMIN = -5.000E-01	XMAX = 0.000E+00		
	YMIN = 0.000E+00	YMAX = 5.000E-01		
	X tic marks at every	5.000E-02		
	Y tic marks at every	5.000E-02		

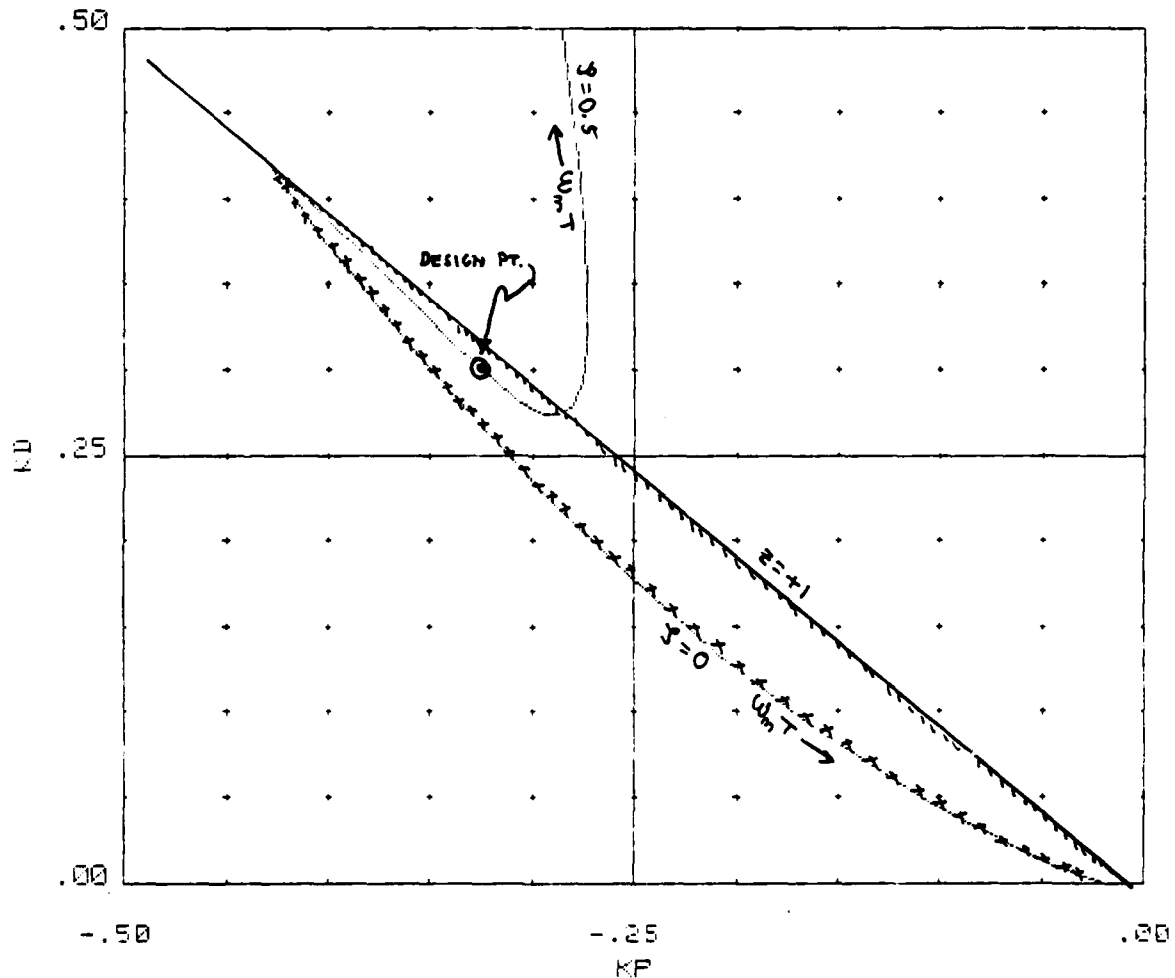


FIGURE 5 Parameter Plane Plot (Enlarged Scale)

If one applies Seltzer's Cross-Multiplication Method³ to Eq. (III-12), one obtains the difference equation,

$$\dot{\theta}(k+1) = \frac{1}{h_3} \left[n_2 \dot{\theta}_c(k) + n_1 \dot{\theta}_c(k-1) + n_0 \dot{\theta}_c(k-2) - h_2 \dot{\theta}(k-1) - h_1 \dot{\theta}(k-2) - h_0 \dot{\theta}(k-3) \right], \quad (\text{III-14})$$

where $\dot{\theta}(k+1)$ indicates the value of $\dot{\theta}(t)$ at the instant of time, $t = (k+1)T$; a value that is held until the next sampling instant, $t = (k+2)T$; etc.

One obvious advantage of SAM is that the form of the reference input, $\dot{\theta}_c(t)$, need not be specified except at the sampling instants. Tables 5 and 6 indicate the missile system's response to unit step and ramp inputs, respectively. They are shown graphically in Figures 6 and 7 .

TABLE 5. COMPUTER PRINT-OUT FOR UNIT STEP RESPONSE

25

ORDER OF NUMERATOR IS 2
SAMPLE INTERVAL = .1

ORDER OF DENOMINATOR IS 3

CALCULATIONS MADE ACCORDING TO FOLLOWING EQUATION DEFINITION

$$C(z)/R(z) = \text{NUMERATOR}/\text{DENOMINATOR}$$

$$\text{NUMERATOR} = A(0)*z^0 + A(1)*z^1 + A(2)*z^2 + \dots + A(N)*z^N$$

$$\text{DENOMINATOR} = B(0)*z^0 + B(1)*z^1 + B(2)*z^2 + \dots + B(D)*z^D$$

NUMERATOR COEFFICIENTS $A(0), A(1), A(2), \dots, A(N)$
3.7064 -3.4164 -.11542

DENOMINATOR COEFFICIENTS $B(0), B(1), B(2), \dots, B(D)$
-4.41246 15.8762 -19.408 8.11889

NUMBER OF STEPS FOR RESPONSE = 30
THE INPUT IS A UNIT STEP FUNCTION

K	TIME	INPUT	RESPONSE
0	0.000E+00	1.000E+00	0.000E+00
1	1.000E-01	1.000E+00	-1.422E-02
2	2.000E-01	1.000E+00	-4.690E-01
3	3.000E-01	1.000E+00	-1.072E+00
4	4.000E-01	1.000E+00	-1.631E+00
5	5.000E-01	1.000E+00	-2.037E+00
6	6.000E-01	1.000E+00	-2.241E+00
7	7.000E-01	1.000E+00	-2.238E+00
8	8.000E-01	1.000E+00	-2.053E+00
9	9.000E-01	1.000E+00	-1.729E+00
10	1.000E+00	1.000E+00	-1.313E+00
11	1.100E+00	1.000E+00	-8.512E-01
12	1.200E+00	1.000E+00	-3.861E-01
13	1.300E+00	1.000E+00	4.967E-02
14	1.400E+00	1.000E+00	4.326E-01
15	1.500E+00	1.000E+00	7.486E-01
16	1.600E+00	1.000E+00	9.921E-01
17	1.700E+00	1.000E+00	1.164E+00
18	1.800E+00	1.000E+00	1.272E+00
19	1.900E+00	1.000E+00	1.324E+00
20	2.000E+00	1.000E+00	1.332E+00
21	2.100E+00	1.000E+00	1.308E+00
22	2.200E+00	1.000E+00	1.264E+00
23	2.300E+00	1.000E+00	1.208E+00
24	2.400E+00	1.000E+00	1.148E+00
25	2.500E+00	1.000E+00	1.092E+00
26	2.600E+00	1.000E+00	1.043E+00
27	2.700E+00	1.000E+00	1.003E+00
28	2.800E+00	1.000E+00	9.732E-01
29	2.900E+00	1.000E+00	9.536E-01
30	3.000E+00	1.000E+00	9.429E-01

NUMBER OF STEPS FOR RESPONSE = 50
THE INPUT IS A UNIT STEP FUNCTION

K	TIME	INPUT	RESPONSE
0	0.000E+00	1.000E+00	0.000E+00

1	1.000E-01	1.000E+00	-1.422E-02
2	2.000E-01	1.000E+00	-4.690E-01
3	3.000E-01	1.000E+00	-1.072E+00
4	4.000E-01	1.000E+00	-1.631E+00
5	5.000E-01	1.000E+00	-2.037E+00
6	6.000E-01	1.000E+00	-2.241E+00
7	7.000E-01	1.000E+00	-2.238E+00
8	8.000E-01	1.000E+00	-2.053E+00
9	9.000E-01	1.000E+00	-1.729E+00
10	1.000E+00	1.000E+00	-1.313E+00
11	1.100E+00	1.000E+00	-8.512E-01
12	1.200E+00	1.000E+00	-3.861E-01
13	1.300E+00	1.000E+00	4.967E-02
14	1.400E+00	1.000E+00	4.326E-01
15	1.500E+00	1.000E+00	7.486E-01
16	1.600E+00	1.000E+00	9.921E-01
17	1.700E+00	1.000E+00	1.164E+00
18	1.800E+00	1.000E+00	1.272E+00
19	1.900E+00	1.000E+00	1.324E+00
20	2.000E+00	1.000E+00	1.332E+00
21	2.100E+00	1.000E+00	1.308E+00
22	2.200E+00	1.000E+00	1.264E+00
23	2.300E+00	1.000E+00	1.208E+00
24	2.400E+00	1.000E+00	1.148E+00
25	2.500E+00	1.000E+00	1.092E+00
26	2.600E+00	1.000E+00	1.043E+00
27	2.700E+00	1.000E+00	1.003E+00
28	2.800E+00	1.000E+00	9.732E-01
29	2.900E+00	1.000E+00	9.536E-01
30	3.000E+00	1.000E+00	9.429E-01
31	3.100E+00	1.000E+00	9.398E-01
32	3.200E+00	1.000E+00	9.425E-01
33	3.300E+00	1.000E+00	9.493E-01
34	3.400E+00	1.000E+00	9.584E-01
35	3.500E+00	1.000E+00	9.685E-01
36	3.600E+00	1.000E+00	9.784E-01
37	3.700E+00	1.000E+00	9.875E-01
38	3.800E+00	1.000E+00	9.951E-01
39	3.900E+00	1.000E+00	1.001E+00
40	4.000E+00	1.000E+00	1.005E+00
41	4.100E+00	1.000E+00	1.008E+00
42	4.200E+00	1.000E+00	1.008E+00
43	4.300E+00	1.000E+00	1.009E+00
44	4.400E+00	1.000E+00	1.009E+00
45	4.500E+00	1.000E+00	1.008E+00
46	4.600E+00	1.000E+00	1.007E+00
47	4.700E+00	1.000E+00	1.006E+00
48	4.800E+00	1.000E+00	1.004E+00
49	4.900E+00	1.000E+00	1.002E+00
50	5.000E+00	1.000E+00	1.001E+00
		1.000E+00	1.000E+00

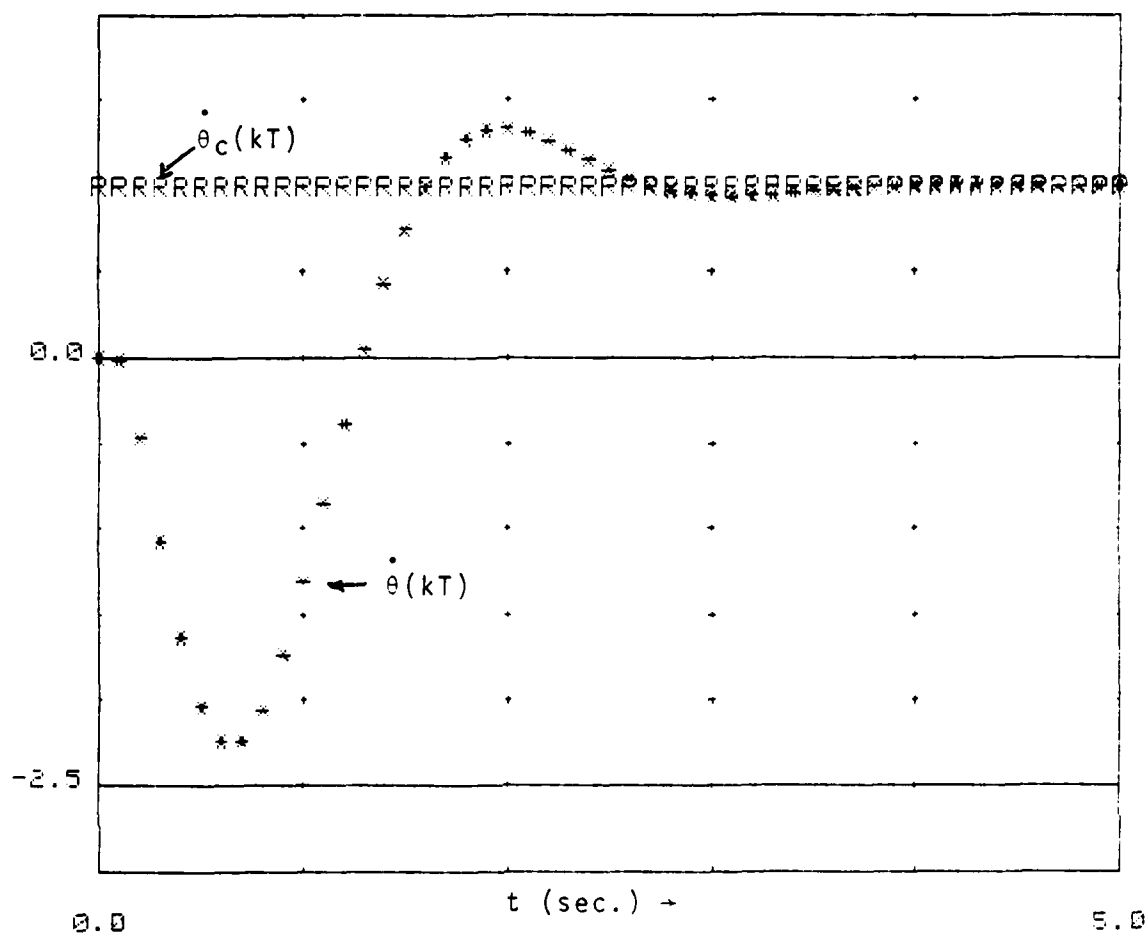


FIGURE 6 Unit Step Response

TABLE 6. COMPUTER PRINT-OUT FOR RAMP RESPONSE

ORDER OF NUMERATOR IS 2
SAMPLE INTERVAL = .1

ORDER OF DENOMINATOR IS 3

CALCULATIONS MADE ACCORDING TO FOLLOWING EQUATION DEFINITION

$$\begin{aligned} C(z)/R(z) &= \text{NUMERATOR}/\text{DENOMINATOR} \\ \text{NUMERATOR} &= A(0)*z^0 + A(1)*z^1 + A(2)*z^2 \dots A(N)*z^N \\ \text{DENOMINATOR} &= B(0)*z^0 + B(1)*z^1 + B(2)*z^2 \dots B(D)*z^D \end{aligned}$$

NUMERATOR COEFFICIENTS A(0), A(1), A(2), ..., A(N)
3.7064 -3.4164 -.11542

DENOMINATOR COEFFICIENTS B(0), B(1), B(2), ..., B(N)
-4.41246 15.8762 -19.408 8.11889

NUMBER OF STEPS FOR RESPONSE = 50

INPUT IS RAMP

SLOPE IS = .1

K	TIME	INPUT	RESPONSE
0	0.000E+00	0.000E+00	0.000E+00
1	1.000E-01	1.000E-02	0.000E+00
2	2.000E-01	2.000E-02	-1.422E-04
3	3.000E-01	3.000E-02	-4.832E-03
4	4.000E-01	4.000E-02	-1.555E-02
5	5.000E-01	5.000E-02	-3.136E-02
6	6.000E-01	6.000E-02	-5.223E-02
7	7.000E-01	7.000E-02	-7.464E-02
8	8.000E-01	8.000E-02	-9.702E-02
9	9.000E-01	9.000E-02	-1.175E-01
10	1.000E+00	1.000E-01	-1.348E-01
11	1.100E+00	1.100E-01	-1.480E-01
12	1.200E+00	1.200E-01	-1.565E-01
13	1.300E+00	1.300E-01	-1.603E-01
14	1.400E+00	1.400E-01	-1.598E-01
15	1.500E+00	1.500E-01	-1.555E-01
16	1.600E+00	1.600E-01	-1.480E-01
17	1.700E+00	1.700E-01	-1.381E-01
18	1.800E+00	1.800E-01	-1.265E-01
19	1.900E+00	1.900E-01	-1.137E-01
20	2.000E+00	2.000E-01	-1.005E-01
21	2.100E+00	2.100E-01	-8.719E-02
22	2.200E+00	2.200E-01	-7.411E-02
23	2.300E+00	2.300E-01	-6.147E-02
24	2.400E+00	2.400E-01	-4.940E-02
25	2.500E+00	2.500E-01	-3.791E-02

26	2.600E+00	2.600E-01	-2.699E-02
27	2.700E+00	2.700E-01	-1.656E-02
28	2.800E+00	2.800E-01	-6.530E-03
29	2.900E+00	2.900E-01	3.202E-03
30	3.000E+00	3.000E-01	1.274E-02
31	3.100E+00	3.100E-01	2.217E-02
32	3.200E+00	3.200E-01	3.157E-02
33	3.300E+00	3.300E-01	4.099E-02
34	3.400E+00	3.400E-01	5.048E-02
35	3.500E+00	3.500E-01	6.007E-02
36	3.600E+00	3.600E-01	6.975E-02
37	3.700E+00	3.700E-01	7.954E-02
38	3.800E+00	3.800E-01	8.941E-02
39	3.900E+00	3.900E-01	9.936E-02
40	4.000E+00	4.000E-01	1.094E-01
41	4.100E+00	4.100E-01	1.194E-01
42	4.200E+00	4.200E-01	1.295E-01
43	4.300E+00	4.300E-01	1.396E-01
44	4.400E+00	4.400E-01	1.497E-01
45	4.500E+00	4.500E-01	1.598E-01
46	4.600E+00	4.600E-01	1.698E-01
47	4.700E+00	4.700E-01	1.799E-01
48	4.800E+00	4.800E-01	1.899E-01
49	4.900E+00	4.900E-01	2.000E-01
50	5.000E+00	5.000E-01	2.100E-01

NUMBER OF STEPS FOR RESPONSE = 100

INPUT IS RAMP

SLOPE IS = .1

K	TIME	INPUT	RESPONSE
0	0.000E+00	0.000E+00	0.000E+00
1	1.000E-01	1.000E-02	0.000E+00
2	2.000E-01	2.000E-02	-1.422E-04
3	3.000E-01	3.000E-02	-4.832E-03
4	4.000E-01	4.000E-02	-1.555E-02
5	5.000E-01	5.000E-02	-3.186E-02
6	6.000E-01	6.000E-02	-5.223E-02
7	7.000E-01	7.000E-02	-7.464E-02
8	8.000E-01	8.000E-02	-9.702E-02
9	9.000E-01	9.000E-02	-1.175E-01
10	1.000E+00	1.000E-01	-1.348E-01
11	1.100E+00	1.100E-01	-1.480E-01
12	1.200E+00	1.200E-01	-1.565E-01
13	1.300E+00	1.300E-01	-1.603E-01
14	1.400E+00	1.400E-01	-1.598E-01
15	1.500E+00	1.500E-01	-1.555E-01
16	1.600E+00	1.600E-01	-1.480E-01
17	1.700E+00	1.700E-01	-1.381E-01
18	1.800E+00	1.800E-01	-1.265E-01
19	1.900E+00	1.900E-01	-1.137E-01
20	2.000E+00	2.000E-01	-1.005E-01
21	2.100E+00	2.100E-01	-8.719E-02
22	2.200E+00	2.200E-01	-7.411E-02
23	2.300E+00	2.300E-01	-6.147E-02

24	2.400E+00	2.400E-01	-4.940E-02
25	2.500E+00	2.500E-01	-3.791E-02
26	2.600E+00	2.600E-01	-2.699E-02
27	2.700E+00	2.700E-01	-1.656E-02
28	2.800E+00	2.800E-01	-6.530E-03
29	2.900E+00	2.900E-01	3.202E-03
30	3.000E+00	3.000E-01	1.274E-02
31	3.100E+00	3.100E-01	2.217E-02
32	3.200E+00	3.200E-01	3.157E-02
33	3.300E+00	3.300E-01	4.099E-02
34	3.400E+00	3.400E-01	5.048E-02
35	3.500E+00	3.500E-01	6.007E-02
36	3.600E+00	3.600E-01	6.975E-02
37	3.700E+00	3.700E-01	7.954E-02
38	3.800E+00	3.800E-01	8.941E-02
39	3.900E+00	3.900E-01	9.936E-02
40	4.000E+00	4.000E-01	1.094E-01
41	4.100E+00	4.100E-01	1.194E-01
42	4.200E+00	4.200E-01	1.295E-01
43	4.300E+00	4.300E-01	1.396E-01
44	4.400E+00	4.400E-01	1.497E-01
45	4.500E+00	4.500E-01	1.598E-01
46	4.600E+00	4.600E-01	1.698E-01
47	4.700E+00	4.700E-01	1.799E-01
48	4.800E+00	4.800E-01	1.899E-01
49	4.900E+00	4.900E-01	2.000E-01
50	5.000E+00	5.000E-01	2.100E-01
51	5.100E+00	5.100E-01	2.200E-01
52	5.200E+00	5.200E-01	2.300E-01
53	5.300E+00	5.300E-01	2.400E-01
54	5.400E+00	5.400E-01	2.499E-01
55	5.500E+00	5.500E-01	2.599E-01
56	5.600E+00	5.600E-01	2.699E-01
57	5.700E+00	5.700E-01	2.799E-01
58	5.800E+00	5.800E-01	2.899E-01
59	5.900E+00	5.900E-01	2.999E-01
60	6.000E+00	6.000E-01	3.099E-01
61	6.100E+00	6.100E-01	3.198E-01
62	6.200E+00	6.200E-01	3.298E-01
63	6.300E+00	6.300E-01	3.398E-01
64	6.400E+00	6.400E-01	3.498E-01
65	6.500E+00	6.500E-01	3.598E-01
66	6.600E+00	6.600E-01	3.698E-01
67	6.700E+00	6.700E-01	3.798E-01
68	6.800E+00	6.800E-01	3.898E-01
69	6.900E+00	6.900E-01	3.998E-01
70	7.000E+00	7.000E-01	4.098E-01
71	7.100E+00	7.100E-01	4.198E-01
72	7.200E+00	7.200E-01	4.298E-01
73	7.300E+00	7.300E-01	4.398E-01
74	7.400E+00	7.400E-01	4.498E-01
75	7.500E+00	7.500E-01	4.598E-01
76	7.600E+00	7.600E-01	4.698E-01
77	7.700E+00	7.700E-01	4.798E-01
78	7.800E+00	7.800E-01	4.898E-01
79	7.900E+00	7.900E-01	4.998E-01
80	8.000E+00	8.000E-01	5.098E-01
81	8.100E+00	8.100E-01	5.198E-01

82	8.200E+00	8.200E-01	5.298E-01
83	8.300E+00	8.300E-01	5.398E-01
84	8.400E+00	8.400E-01	5.498E-01
85	8.500E+00	8.500E-01	5.598E-01
86	8.600E+00	8.600E-01	5.698E-01
87	8.700E+00	8.700E-01	5.798E-01
88	8.800E+00	8.800E-01	5.898E-01
89	8.900E+00	8.900E-01	5.998E-01
90	9.000E+00	9.000E-01	6.098E-01
91	9.100E+00	9.100E-01	6.198E-01
92	9.200E+00	9.200E-01	6.298E-01
93	9.300E+00	9.300E-01	6.398E-01
94	9.400E+00	9.400E-01	6.498E-01
95	9.500E+00	9.500E-01	6.598E-01
96	9.600E+00	9.600E-01	6.698E-01
97	9.700E+00	9.700E-01	6.798E-01
98	9.800E+00	9.800E-01	6.898E-01
99	9.900E+00	9.900E-01	6.997E-01
100	1.000E+01	1.000E+00	7.097E-01

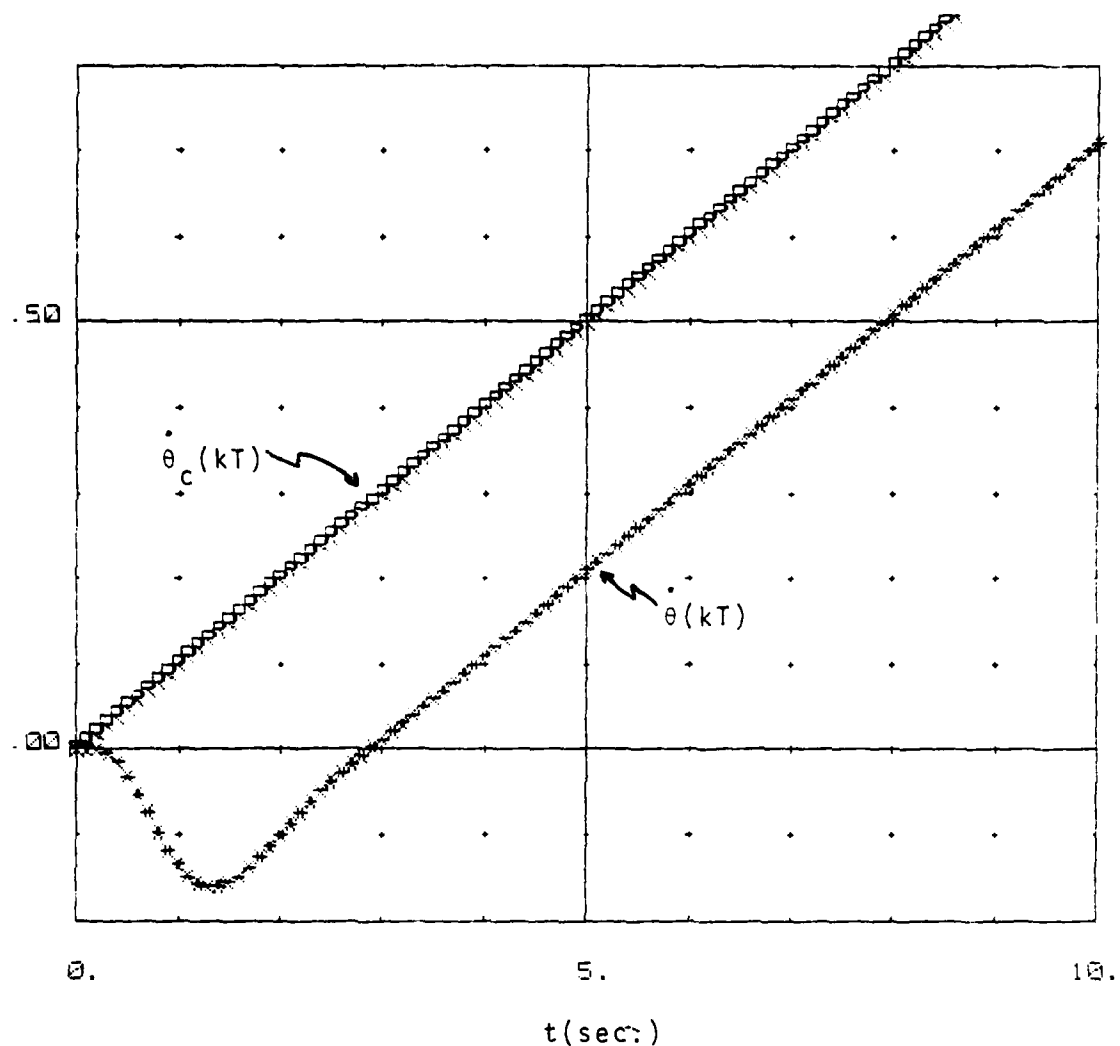


FIGURE 7 Ramp Response

SECTION IV. CONCLUSIONS

The planar equations of motion have been developed for the FAMMS missile system. They were linearized to permit stability and preliminary autopilot design to proceed. A technique for performing this preliminary design has been developed and applied. In the actual case, the design would be repeated until a near-optimal design was achieved. It would then be repeated for several linearized operating points along the path of a nominal trajectory. Then the system would be "flown" on a simulation with numerical values for autopilot coefficients changed during flight if necessary. Finally, the procedure would be repeated for three-dimensional equations of motion.

APPENDIX A. DETERMINATION OF DIGITAL CONTROL SYSTEM RESPONSE
BY CROSS-MULTIPLICATION

The following material was developed under US Army Missile Command Contract DAAK40-78-C-0226 and completed under this contract (DAAH01-81-M-A118). It was accepted and presented at the IEEE Region 3 "SOUTHEASTCON '81" Conference held in Huntsville, Alabama on 5-8 April 1981.

DETERMINATION OF DIGITAL CONTROL SYSTEM RESPONSE BY CROSS-MULTIPLICATION

SHERMAN M. SELTZER

Control Dynamics Company
Huntsville, Alabama

ABSTRACT

This paper describes the Cross-Multiplication technique for obtaining the response of a digital control system from its closed-loop transfer function. When the latter is expressed in the complex z-domain, the response may be obtained at the sampling instants. If it is desired to know the response between the sampling instants, the Submultiple Method may be adapted to the Cross-Multiplication technique. When the transfer function is expressed in the Modified z-transform domain, the response is obtained at any point within each sampling instant. The three approaches are described and applied to an example.

I. INTRODUCTION

This paper describes a technique for obtaining the response of a digitally controlled system. It is assumed that the closed-loop transfer function is available in the z-or modified z-transform domain. The numerator and denominator of each side of the transfer function are cross-multiplied. The Real Translation Theorem is then applied to the result, yielding a difference equation in the time-domain. This may be solved for the system response in terms of the reference (or other) input(s) to the system as well as in terms of system state initial conditions. Two different modifications to the basic technique are described: one using the submultiple method and one using the modified z-transform technique. These are applied when it is desired to determine intra-sampling responses of the system. All three techniques are applied to a single example. A summary of the techniques and their application is provided at the conclusion of this note.

This work was supported by the US Army Missile Command under Contract DAAK40-78-C-0226.

II. RESPONSE AT SAMPLING INSTANTS

It is assumed that a given digital or sampled-data system can be described by a closed-loop transfer function that relates the controlled output of the system to the reference input. If there is more than one input, the technique can also be applied to the resulting sum of closed-loop transfer functions relating the controlled output to each of the inputs. Although this note refers only to a single controlled output, the technique can be applied to find any system state if it is related to the inputs to the system in the z-domain.

It is assumed that the state whose response is desired is denoted in the z-domain as $C(z)$ and the reference input as $R(z)$. The relationship between $C(z)$ and $R(z)$ usually can be expressed as a closed-loop transfer function (or several such transfer functions) which is a ratio of two polynomials in z , i.e.,

$$\frac{C(z)}{R(z)} = \frac{\sum_{j=0}^M a_j z^j}{\sum_{k=0}^N b_k z^k}, \quad (1)$$

where coefficients a_j and b_k represent the system parameters. The procedure for finding the response at sampling instants--by the cross-multiplication method--consists of three steps. First one cross-multiplies the numerators with the denominators of Equation (1). Then each term of the resulting expression is divided by $b_N z^N$. This result is solved for the $C(z)$ term that is not multiplied by a nonzero power of z , i.e.

$$C(z) = \frac{1}{b_N} \left[\sum_{k=0}^M a_k z^{k-N} R(z) - \sum_{j=0}^{N-1} b_j z^{j+1} C(z) \right] \quad (2)$$

Finally, the Real Translation Theorem is applied to Equation (2). The resulting values of $c(nT)$ at each sampling instant, nT , become

$$c(nT) = \frac{1}{b_N} \left\{ \sum_{k=0}^M a_k r[(n-N+k)T] - \sum_{j=0}^{N-1} b_j c[(n-N+j)T] \right\} \quad (3)$$

where j, k, M, N , and n are integers.

The advantages of the form of Equation (3) are three-fold: (1) the value of $c(nT)$, for any $t=nT$, may be obtained for any form of $r(t)$, whether or not it is "z-transformable;" (2) the expression for $c(nT)$ does not have to be recalculated every time the form of $r(t)$ changes, as is the case when the response is determined by the partial fraction, power series, or inversion formula methods; and (3) the form of the expression for $c(nT)$ permits the inclusion of initial conditions, such as $c(0)$, if they exist.

III. RESPONSE BETWEEN SAMPLING INSTANTS: SUBMULTIPLE METHOD

If it is desired to find the intra-sampling response of the same type sampled-data system described in Section II, it may be accomplished by applying the submultiple method.¹ Briefly, let $c(mT/n)$ represent the value of the response $c(t)$ at the instant, $t=mT/n$, where $n-1$ represents the number of intrasampling responses desired (n is an integer with value greater than unity). If m is an integer, the sampling period within which the submultiples are to be determined is denoted as mT . The z-transform of $c(mT/n)$ may be found from the ordinary z-transform in the following manner. In essence, $c(mT/n)$ is the output of a fictitious sampler which samples n times as fast as the real sampler. The z-transform of that output is defined as

$$\mathcal{Z}\{c(nT/m)\} \underset{\substack{z \rightarrow z_n \\ T \rightarrow T_n}}{=} C(z)_n = C(z) \quad (4)$$

where $z=z^{1/n}$ and $T=T/n$. Now the closed-loop expression of Equation (1) may be altered to read

$$\frac{C(z)_n}{R(z)} = \frac{\sum_{j=0}^M a_j z_n^j}{\sum_{k=0}^N b_k z_n^k}. \quad (5)$$

The submultiple modification to the basic method also consists of three steps which are analogous to the steps of Section II. The result is the expression

$$c(mT/n) = \frac{1}{b_N} \left\{ \sum_{k=0}^M a_k r[(m-N+k)T/r] - \sum_{j=0}^{N-1} b_j c[(m-N+j)T/r] \right\} \quad (6)$$

where all values of $r[\cdot]$ are equal to zero except for those values of $r[\cdot]$ at integral multiples of T , at which time $r(pT)$ equals the value of $r(t)$ at $t=pT$; j,k,M,m,N,n,p are integers.

IV. RESPONSE BETWEEN SAMPLING INSTANTS: MODIFIED Z-TRANSFORM METHOD

If it is desired to find the intra-sampling response of the same type of sampled-data system described in Section II, it also may be accomplished by applying the modified z-transform

method.¹ In this method it is necessary first to determine the modified z-transform equivalent of the closed-loop transfer function of Equation (1), i.e.

$$\frac{C(z,m)}{R(z)} = \frac{\sum_{j=0}^M a_j z^j}{\sum_{k=0}^N b_k z^k} \quad (7)$$

where a_j and b_k may be functions of m . The cross-multiplication technique is similar to those two previously described. Again, the numerators and denominators of Equation (7) are cross-multiplied. Each term is divided by $b_N z^N$, and the resulting equation is solved for the $C(z,m)$ term that is not multiplied by a non-zero power of z . The inverse z-transform of each term is determined, yielding

$$c[(n-1)T,m] \equiv c[(n-1+m)T] \quad (8)$$

$$= \frac{1}{b_N} \left\{ \sum_{j=0}^N a_j r[(n-N+j)T] - \sum_{k=0}^{N-1} b_k c[(N-1+m-N+k)T] \right\}$$

where i,k,M,m,N are integers.

V. EXAMPLE

Given the closed-loop sampled-data system shown in the figure, where $G(s)=1/s(s+1)$ and $H(s)=1$. The closed-loop transfer function is found to be

$$\frac{C(z)}{R(z)} = \frac{(1-e^{-T})z}{z^2 - 2e^{-T}z + e^{-T}} \quad (9)$$

Applying the three steps prescribed in Section II, one may obtain

$$c(nT) = (1-e^{-T})r[(n-1)T] + 2e^{-T}c[(n-1)T] - e^{-T}c[(n-2)T]. \quad (10)$$

Now values for the response may be found at the sampling instants by letting n progressively take on values of $0, 1, 2, \dots$

If it is desired to find the response between sampling instants by the submultiple method, it may be shown that

$$C(z)_n = G(z)_n E(z) = G(z)_n R(z) / [1+HG(z)], \quad (11)$$

where $G(z)_n$ is found by the means shown in Equation (4). Application of the procedures of Section III yields the time-domain difference equation for $c(t)$ at the instant of time, $t=mT/n$, where m is any desired integer. A fictitious time delay, $e^{-(1-m)T}$, may be placed following the forward loop gain, $G(s)$, and a fictitious time advance (of the same magnitude) may be placed just before the feedback

loop gain $H(s)$. The closed-loop transfer function that results from these two elements being added is

$$\frac{C(z,m)}{R(z)} = \frac{G(z,m)}{1 + HG(z)} = \frac{(1-e^{-mT})z + (e^{-mT}-e^{-T})}{z^2 - 2e^{-T}z + e^{-T}} \quad (12)$$

It may be observed that Equation (12) is in the same form as Equation (7). Hence the prescribed operations of Section IV may be applied, resulting in the difference equation

$$\begin{aligned} c[(n-1+m)T] &= (1-e^{-mT})r[(n-1)T] + (e^{-mT}-e^{-T}) \\ &\cdot r[(n-2)T] + 2e^{-T}c[(n-2+m)T] - e^{-T} \\ &\cdot c[(n-3+m)T]. \end{aligned} \quad (13)$$

During the n th sampling period, i.e. $(n-1)T \leq t \leq nT$, where n is an integer, one lets m assume values between zero and one to find the intrasampling values of $c(T)$.

VI. CONCLUSIONS

Several analytical techniques for obtaining the response of a digital control system have been described. They are based on a single principle: cross-multiplication followed by applications of the real translation theorems. Each is applied to a single example. As a starting point for application of each of the techniques, it is required that the dynamics of the digital control system be described in the z - or modified z -domain.

The advantages of the three techniques over extant classical methods are:

The response may be obtained for any deterministic reference input into the system as long as its value is known at the sampling instants. It need not be described by a differential equation, and the z -transform for a specific reference input need not be determined before obtaining an expression for the response.

Initial conditions and instantaneous changes can be accommodated readily by the equations obtained through use of the cross-multiplication methods.

The difference equations obtained are particularly amenable to programming on a desktop calculator or digital computer.

A detailed knowledge of the theory underlying digital or sampled-data control systems is not required (although it certainly is helpful) by the analyst in order to apply the recipes described herein.

REFERENCE

¹B.C. Kuo, *Analysis and Synthesis of Sampled-Data Control Systems*, New Jersey, Prentice-Hall, 1963.

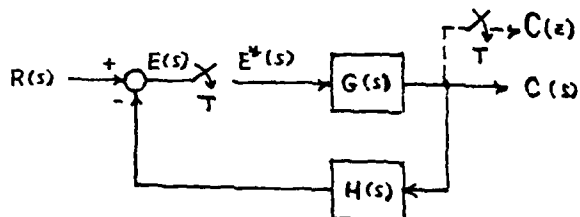


Figure. Closed-loop sampled-data system

**APPENDIX B. A VALIDATED METHODOLOGY FOR ACCURATELY PREDICTING
MISSILE FLIGHT PERFORMANCE**

The following material was developed in part and completed under this contract (DAAH01-81-MA118). It was accepted and presented at the American Astronautical Society Annual Rocky Mountain Guidance and Control Conference at Keystone, Colorado on 31 January - 4 February 1981.

AAS 81-004



A VALIDATED METHODOLOGY FOR ACCURATELY PREDICTING
MISSILE FLIGHT PERFORMANCE

HAROLD L. PASTRICK, US ARMY MISSILE COMMAND
SHERMAN M. SELTZER, CONTROL DYNAMICS COMPANY

ANNUAL ROCKY MOUNTAIN GUIDANCE AND CONTROL CONFERENCE

January 31 through February 4, 1981
Keystone, Colorado

Sponsored by
ROCKY MOUNTAIN SECTION
AMERICAN ASTRONAUTICAL SOCIETY

A detailed black and white line drawing of a mountainous landscape. In the foreground, there is a dense forest of tall evergreen trees. Behind the forest, several rugged mountain peaks rise, with some showing signs of snow or ice. The sky above the mountains is clear and blue.
AAS PUBLICATIONS OFFICE, P. O. BOX 28130 - SAN DIEGO, CALIFORNIA 92128

A VALIDATED METHODOLOGY FOR ACCURATELY PREDICTING MISSILE FLIGHT PERFORMANCE

Harold L. Pastrick* and Sherman M. Seltzert

A comprehensive hardware-in-the-loop (HWIL) simulation has been developed, operational in real-time, to perform guidance and control system design verification and autopilot and detector optimization for a laser semiactive terminal homing weapon system. Emphasis was placed on the development of time-critical aspects of the simulation including analog-digital computer partitioning, aerodynamic moment updating, and target-vehicle geometry modeling. Validity of the simulation was demonstrated by comparing results obtained from the all-digital 6-DOF and hybrid analog-digital simulations. The simulation was proven an invaluable evaluation and optimization tool in efforts to enhance weapon system performance, since simulation results were indicated by actual flight tests.

INTRODUCTION

It is a widely accepted principle in the missile development community that the ultimate figure of merit for a missile is its performance in flight. Typically, a significant amount of dollars is dedicated to the flight test phase of the development program in order to assess its strengths and shortcomings in scenarios ranging from simplistic (advanced development concepts) to battlefield conditions [Operational Testing (OT) under an emulated realistic environment]. To the extent that key missile parameters are monitored, the principle of flight testing remains as the soundest indicator of missile system performance.

However, it is not unusual to have a missile fail in a flight test. Thus it would yield little or no data for reasons such as telemetry failure, camera coverage inadequacies or planned nonmonitoring of parameters as is the condition for OT flights. A variety of reasons such as these and others, to yield flight equivalent data, motivates the search for an alternative to flight testing. At the US Army Missile Command (MICOM), that alternative is widely accepted under the name of hardware-in-the-loop (HWIL) simulation testing.¹ In this mode of simulation, actual

*Chief, Guidance and Control Analysis, Guidance and Control Directorate, US Army Missile Laboratory, US Army Missile Command, Redstone Arsenal, Alabama 35898.

¹Consulting Engineer, Control Dynamics Company, 221 East Side Square, Suite 1B, Huntsville, Alabama 35801.

missile flight hardware such as autopilot, actuator, seeker, inertial components and flight computer are included in a simulation that is closed around a digital/analog computer that has been coded with appropriate models to yield an emulated flight in real-time.²

The intent of this paper is to summarize the concept of HWIL simulation testing as performed within several elements of MICOM and display the correlation of those tests (which are nominally nondestructive) to flight tests. In particular, data will be provided to show that hundreds of preflight runs in a well-designed HWIL test not only predict flight performance to within 3 sigma tolerances, but actual HWIL simulation tested hardware performs better in flight because of the advantage of having been "tweaked-to-perfection" in the simulation laboratory.³ This does not imply that perfection has been achieved via simulation. To the contrary, as the example of "lessons learned" has shown.⁴ Post-flight analysis of two early guided projectiles indicated aerodynamic maneuverability was less than that predicted by wind tunnel tests and, of course, those aero data were incorporated in the simulation models. The cause, effect, and solution will be discussed. Nevertheless, savings in the millions of dollars have been demonstrated by virtue of using the HWIL simulation testing as a precursor to flight test.⁵

SIMULATION EVOLUTION

The Guidance and Control Directorate of the US Army Missile Laboratory, MICOM, has been engaged for a number of years in the area of semiactive laser terminal homing guidance. In essence, this type of guidance consists of designating the target by a ground-based laser beam and using a missile-mounted laser receiver/detector, in the terminal phase of the missile's flight, to provide guidance and control signals by tracking the laser energy reflected by the target.

As part of the advanced development effort applied to this research area, an extensive program of simulation studies was undertaken to identify potential problem areas and to indicate approaches to their solution. The initial approach consisted of a full six degree-of-freedom (6 DOF) digital computer-based simulation which focused on the effects upon missile performance of variations in autopilot design during the evolution of the missile's configuration.

The next stage in the simulation activity took place over a longer period and was related to the choice of the guidance and control system and optimization of the guidance law and autopilot mechanization. Amendments and improvements were made to the simulation as new data (aerodynamic coefficients, hardware parameters, etc.) became available. It was, however, realized that the models employed were idealized and suffered limitations in their representation of the real world. In an attempt to overcome some of the more obvious limitations, test results from an early version of the laser seeker were included in the simulation in place of the idealized seeker model; the test results involved the introduction of Gaussian noise, thus requiring a Monte Carlo approach to obtaining results.

Further efforts to investigate and validate the guidance and control system were directed to a time frame immediately after the design stage was complete, when prototype hardware had been produced but prior to initial flight tests of the missile. The method selected was a natural extension of the earlier simulation work and consisted of a hybrid digital-analog real-time computer simulation employing the guidance and control HWIL. This was considered an important part of the development phase because, although the hardware had been manufactured, it was still possible to vary a number of the design parameters, and in addition optical-gimbal coupling in the seeker was recognized as a problem which was difficult to handle theoretically. Furthermore, closed loop operation in a realistic simulation offered the opportunity of studying the dynamic stability and performance of the hardware system first hand, with the hope of reducing the length and cost of the flight testing cycle.

HARDWARE-IN-THE-LOOP SIMULATION OVERVIEW

The hybrid simulation facility consists of the major components shown in Fig. 1. The interfaces contain the hybrid input/output and communication devices which include analog-digital converters (ADC's), multiplying digital-analog converters (MDAC's), discrete digital input/output lines, interrupt lines, and real-time clocks.

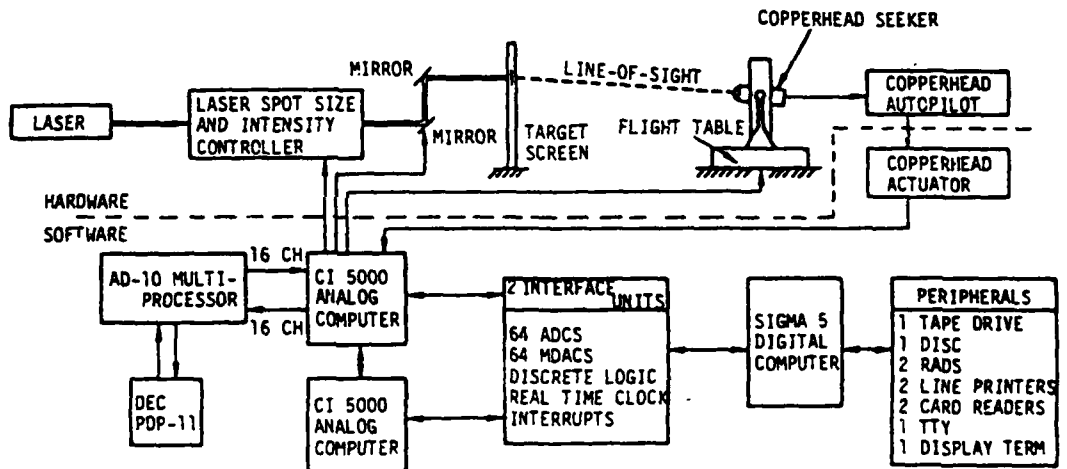


Fig. 1 Block Diagram of hardware-in-the-loop (HWIL) simulation facility.

The digital computer configuration contains an extensive array of peripheral devices including disk files, a tape drive, and a graphics display terminal. A set of 16 priority external interrupts is included in the system; these may be triggered by events which occur on the analog computers or internally by the digital program. The analog computers are 100-V solid-state machines and both contain a wide range of linear, non-linear, and logic elements.

The laser target simulator consists of a neodymium YAG pulsed laser beam which is reflected onto a translucent screen by a plane mirror; the mirror

has two gimballed rotational degrees of freedom about perpendicular axes approximately in the plane of the mirror. Rotation of the mirror about these axes permits the laser spot to be positioned any point on the screen. Mirror rotational positions are servo-controlled with input voltages derived from either the analog or digital simulators. Laser spot size and energy density are controllable by a variable position lens placed at the laser generator output. During a simulation run, using the real laser sensor in the loop, the laser spot is positioned on the screen such that the actual line-of-sight angles to the target as seen by the missile are reproduced. The effect of range closure between missile and target is simulated by varying the laser spot size and energy density.

The rotational motion simulator consists of a three-axis electrohydraulic, gimballed flight table controlled by angular position inputs. It is used to simulate the missile angular motion experienced by the G&C hardware components. The flight table is placed so that the laser seeker component of the guidance hardware, when mounted on the flight table, is able to sense the laser spot through the translucent screen; the latter acts to diffuse the laser spot in a manner similar to that produced by a real target.

For the purpose of partitioning the mathematical models into digital and analog sections, the models were considered in the following groups:

- 1) Group a - This group contained the missile dynamics and was divided between the digital and analog machines with the translational equations and aerodynamic table interpolations on the digital computer. This took advantage of the wider dynamic range of the digital machine and recognized that the translational equations had the lowest frequency content. The rotational equations were assigned to the analog machine because the anticipated rotational frequencies required integration rates not attainable in the time available to the digital computer when operating in real-time. However, the applied aerodynamic moment inputs to the rotational equations were generated on the digital computer because of the necessity of interpolating in tabulated functions of two and three independent variables.
- 2) Group b - This group contained the target position and calculation of missile-target miss distance at intercept and was assigned exclusively to the digital computer because of the need for maximum accuracy in the miss distance calculation and its association with the missile translation equations.
- 3) Group c - With the exception of the seeker sample-hold detector, Group c was assigned to the analog machines since these models contained the highest frequency content in the simulation. The seeker sample-hold output was generated on the digital computer because it depended on relative translational displacement of the missile and target. In addition, however, the gyro model was duplicated in the digital computer to generate accurate gimbal angles for the calculation of detector sample-hold output. It was found that unacceptable errors were introduced in the transformation of missile-target displacement to seeker axes if the seeker angle were obtained by analog-digital conversion of analog outputs because of

the small values over a large part of the flight range. Figs. 2 and 3 show the digital and analog program in block diagram form.

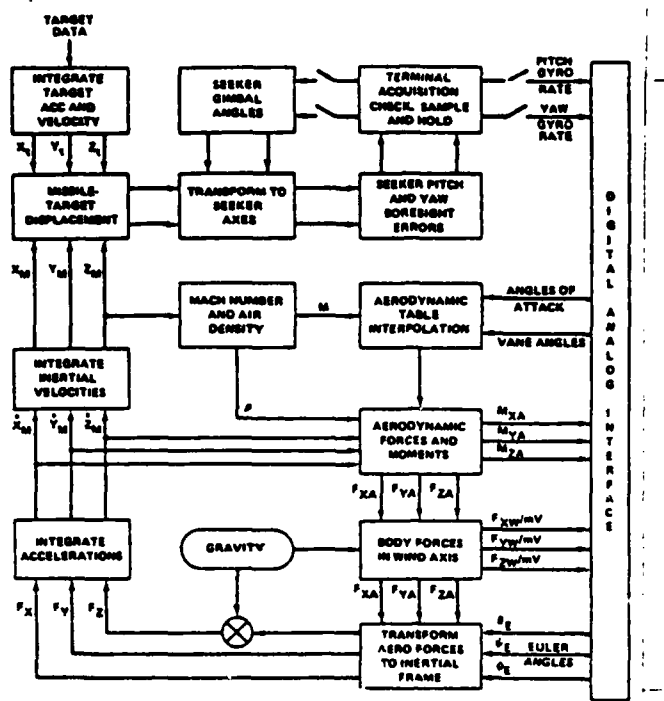


Fig. 2 Block diagram of the digital section of the simulation.

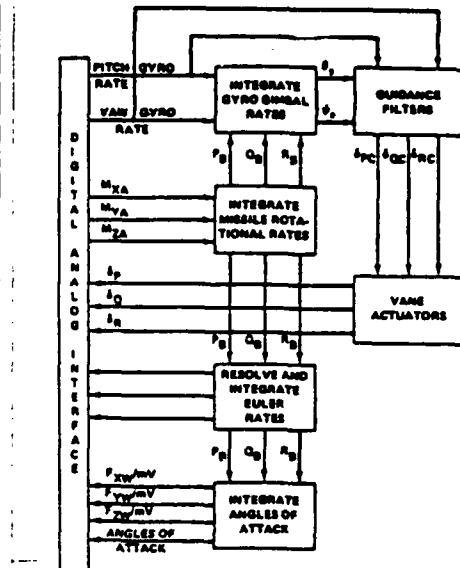


Fig. 3 Block diagram of the analog section of the simulation.

To insure that the simulation system was operating satisfactorily, two dynamic tests were performed. The analog results from these tests were compared with results taken from an all-digital simulation and a Continuous System Simulation Language (CSSL) modular digital simulation. The procedure for conducting the test and interpreting the results is shown as follows. Test No. 1 provides a dynamic check on the following variables: δp (roll vane), δQ (pitch vane), δR (yaw vane), θ_s (pitch gyro), ψ_s (yaw gyro), θ_R (pitch roll rate gyro), and ψ_R (yaw roll rate gyro). The procedure is to: (1) place an IC on the following variables: P , Q , R , W_y , and W_z ; (2) set $D_P = D_Q = D_R = 0$; and (3) set control lines via the Digital-to-Analog Converter (DAC). Test No. 2 provides a dynamic check on the following variables: P (roll body rate), Q (pitch body rate), R (yaw body rate), ϕ (roll Euler angle), θ (pitch Euler angle), ψ (yaw Euler angle), α (pitch angle of attack), and β (yaw angle of attack). This was done in the same manner as Test No. 1. Fig. 4 presents highlights of the results of the method. For flight test, the model, scenario, and flight parameters require further discussion.

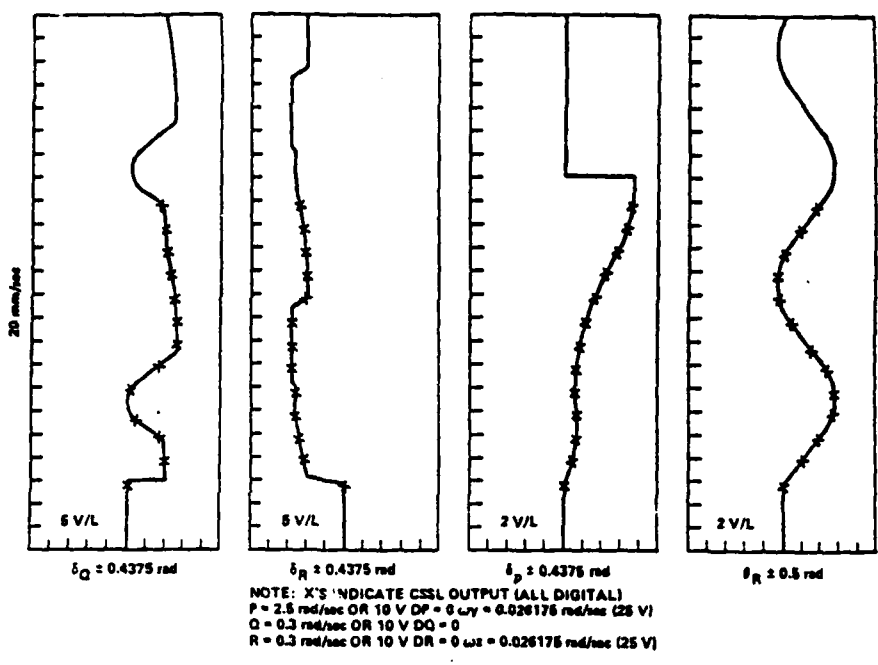


Fig. 4 Digital and analog test results (Test No. 1).

WEAPON SYSTEM CONCEPT

Army artillery has been used as an effective weapon for saturation fire upon area targets in the past; however, the artillery barrage has been lacking in capability to destroy a point target. Because the armored moving target was deemed difficult to kill and because it usually required a direct hit to immobilize it, studies concluded that a new weapon had to be developed to meet this threat. It was suggested that the ultimate mission of the new weapon system would be to enhance the indirect fire capability by disrupting, delaying, disorganizing, and destroying enemy mechanized forces before and during the time they were engaged by direct fire weapons. Thus, the 155-mm howitzer with laser semiactive homing guided munitions was conceived. The munition itself is now commonly called COPPERHEAD (CLGP) -- Cannon Launched Guided Projectile.

The COPPERHEAD CLGP design is predicated on its intended use in a tactical situation. The typical trajectory shown in Fig. 5 depicts the launch, midcourse, and terminal homing phases. The high-g launch is shown immediately after which the stabilizing fins are deployed. On the ballistic trajectory the mechanism for guidance and control is uncaged. After uncaging, target acquisition can occur; that is, the laser energy reflected from the target can be acquired by the sensor mechanism. Once the target has been acquired by the sensor, guidance can begin. The guidance problem, in which the heading error is nulled, begins when acquisition is achieved. (The heading error is defined as the angle between the line of sight to the target and the velocity vector of the projectile.) When the heading error has been nulled, the end game begins wherein the guidance system overcomes disturbances such as those due to wind or target motion (see Fig. 6 for a simplified one-axis block diagram).

(6)

Fig. 5 Projectile sequencing and phases.

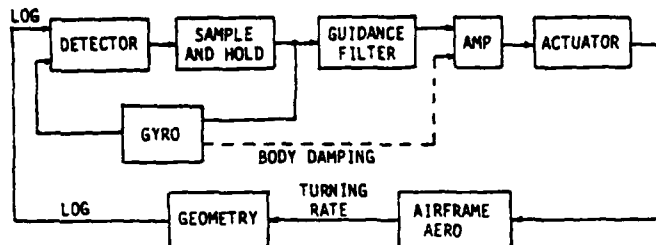
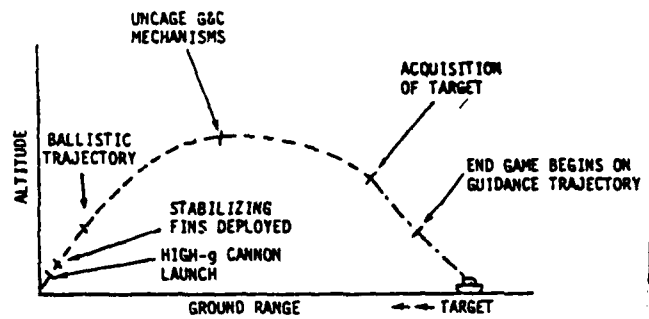


Fig. 6 One-axis block diagram.

The COPPERHEAD projectile (Fig. 7) is 155 mm in diameter and 4.5 ft long, and weighs 138 lb. The projectile nose is a blunted conical dome. Aft of the dome is a primary optical lens bonded to a detector assembly. The detector assembly contains other optics, a laser detector, and video preamps. The detector and primary lens assembly are attached to a coil form that contains both torquing and spin-sustain coils for the seeker gyro.

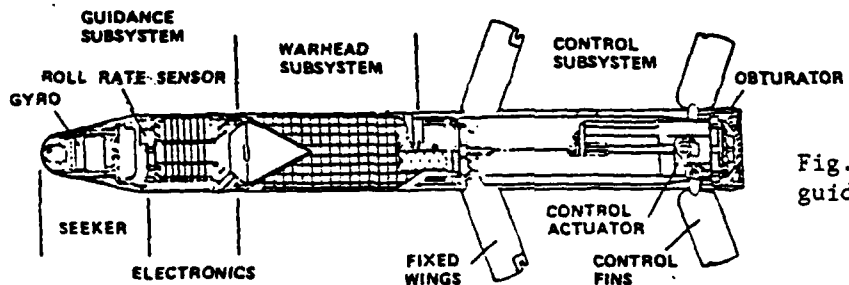


Fig. 7 COPPERHEAD guided projectile.

A two-axis gimballed gyro using load transfer bearings and a "gotcha" sleeve, which engages the gyro rotor during launch for launch survivability, are housed inside the coil form assembly. These items carry the large loads incurred during cannon launch and protect the gimbal bearings from brinelling. The gyro rotor has a mirror surface to reflect laser energy onto the detector and incorporates a magnetic ring that enables the gyro to be precessed or spun when the torquing or spin coils are energized. Initial spinup for the seeker gyro is provided by a wound spring.

The projectile electronics package located behind the seeker gyro section consists of eight printed-circuit cards plugged into a motherboard

assembly. The launch loads induced on the seeker gyro section and the electronics package are carried by the steel electronics housing that mechanically interfaces with the warhead subsystem. The electronics housing also incorporates a forward bourrelet, which acts as a bore rider during travel down the gun tube. An unconventional roll rate sensor is mounted on the forward bulkhead of the electronics package.

The steel warhead structure contains a shaped-charge warhead, warhead fuse with safe and arm (S&A) provisions and interconnecting electrical cables for interfacing the guidance subsystem with the control subsystem. During early testing, a telemetry unit having representative mass and envelope characteristics of the warhead is substituted for the warhead.

The control housing contains slots that permit the fins and fixed wings to be folded inside the structure during storage and cannon launch. Actuator electronics, thermal battery, and a cold-gas storage bottle for the controls are mounted on the control actuator unit. The actuator assembly is held in the control housing by an aft closure, which also incorporates the projectile's obturator. The control section also contains locks which hold the fins and wings inside the structure and a cam/piston mechanism which deploys the wings upon command.

HARDWARE-IN-THE-LOOP

Test Setup

The HWIL simulation is performed on the MICOM Guidance and Control Analysis group's terminal homing guidance evaluation facility. For HWIL operation it is necessary for the seeker to experience the projectile angular orientation and to sense the target-projectile relative translational displacements. This is achieved by mounting the hardware seeker on a three-axis flight table to enable the body-inertial Euler angles for generation in real-time while sensing the laser energy projected onto a translucent screen to simulate the target. The target spot is deflected via mirror and bellow interfaces to represent the line-of-sight change between the target and projectile and include the effects of relative range closure between them. Models of the airframe, actuator, gyro, seeker, and compensation networks are required with the mathematical generation of three flight table angles, two laser mirror angles, and aperture settings for the laser lens. Fig. 8 highlights the system features.

Briefly, the test sequence consists of securing the seeker guidance module to the three-axis flight table connecting cables, to the test monitor breakout box, and to the computer's interface. Voltage levels and polarities are checked at the initial power-up condition. Simulated flights for a prescribed target are seen against a variable laser setting to simulate range closure by increasing the laser energy transmitted to the seeker via the bellows on the laser simulator. Groups of five runs each quantify the total range of the seeker from maximum range at detection (lowest energy at acquisition) to maximum energy (impact condition). Finally, orientations of the seeker in various roll positions are made to values of 45, 90, and 180 deg. If deemed necessary to improve miss

distance, vane effectiveness is improved via settings on the analog machine, and g bias is increased via an amplifier gain on the analog. A group of runs in each of these conditions may require 60 to 100 trials. These are all oriented to maximizing performance prior to flight testing at White Sands Missile Range.

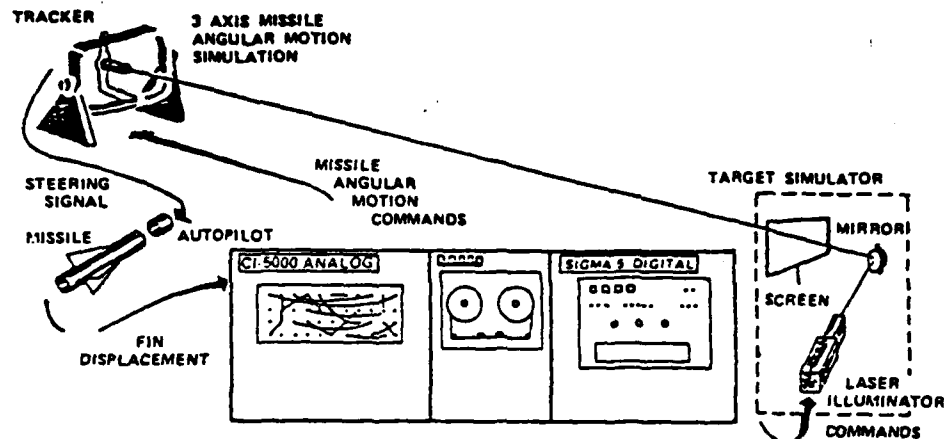


Fig. 8 Hardware-in-the-loop simulation.

Early Test Results

A set of results from the hybrid simulation is shown in Figs. 9 through 11. These are given in the form of strip chart outputs showing the variation of parameters over the terminal homing portion of the missile trajectory, and were obtained with a target located 12,500 ft downrange from the missile at the time of acquisition. Miss distance, normalized by the circular error probability, was 0.45 ft.

As soon as the hybrid real-time simulation was performing satisfactorily, the guidance hardware components were inserted into the simulation loop. Initial experience immediately highlighted several problem areas which had not been discovered in the early open-loop hardware tests. Most prominent of these included poor automatic gain switching in a set of log-amps in the combined seeker detector and the gyro torquer loop.

A set of results from the HWIL simulation, for the same target conditions as given for the hybrid simulation results, is shown in Figs. 12 through 14. Normalized miss distance was 0.73 ft. Comparison of these two sets of results shows the inability of the simplified models to represent the actual hardware in detail when high frequency noise is generated. However, the low frequency fidelity was consistently good.

Optimization of various hardware parameters with respect to missile target miss distance at intercept was then attempted. These parameters included navigation ratio, gyro rotor speed, range on entry to terminal homing, vane effectiveness, and optical-gimbal coupling. Optimization methodology consisted of choosing nominal parameter values, performing a set of five

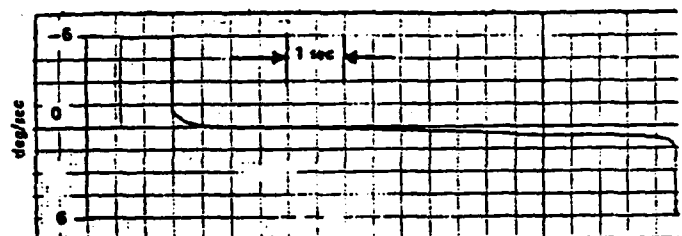


Fig. 9 Hybrid simulation pitch channel sample-hold output (gyro pitch rate).

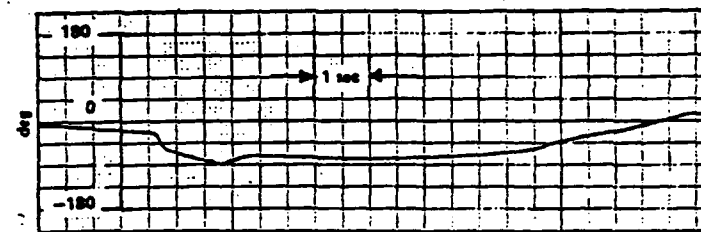


Fig. 10 Hybrid simulation pitch axis Euler angle θ_E .

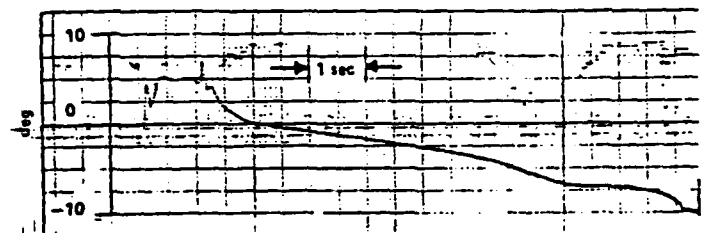


Fig. 11 Hybrid simulation pitch channel vane angle.

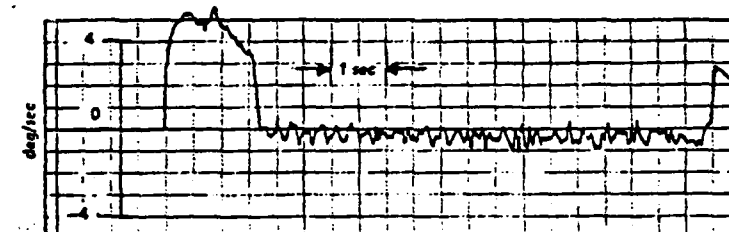


Fig. 12 Guidance HWIL pitch channel sample-hold output.

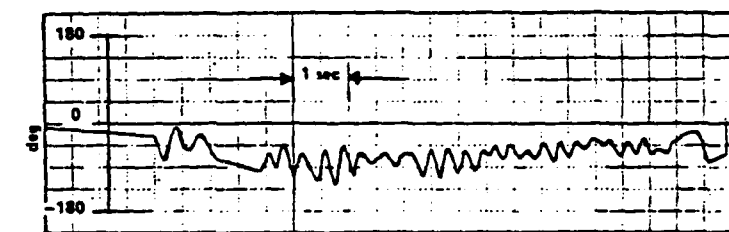


Fig. 13 Guidance HWIL pitch axis Euler angle θ_E .

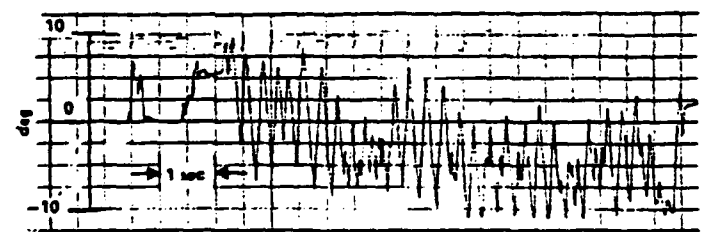


Fig. 14 Guidance HWIL pitch vane angle.

simulation runs to give an average miss distance and graphing the miss distance against the parameter to give an average miss distance and graphic the miss distance against the parameter to give the optimum value as a minimum on the curve. Several optimization results are given in Figs. 15 and 16. Note that miss distances are averaged over five runs and expressed in a form normalized by the circular error probability. In Figs. 15 and 16 the parameters not being optimized were held at their nominal values. Obviously, the overall optimization procedure required several iterations because coupling existed between many of the various parameters.

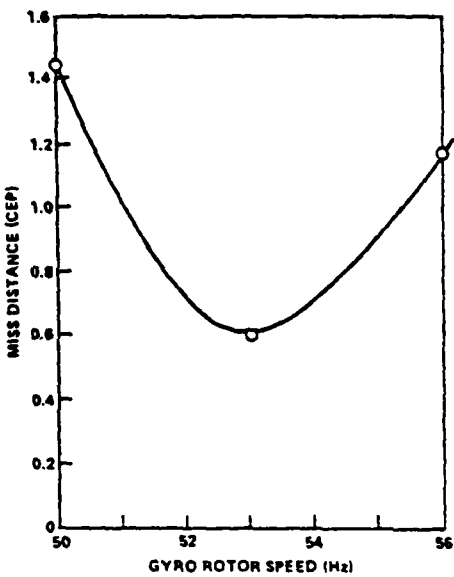


Fig. 15 Miss distance as a function of gyro rotor speed.

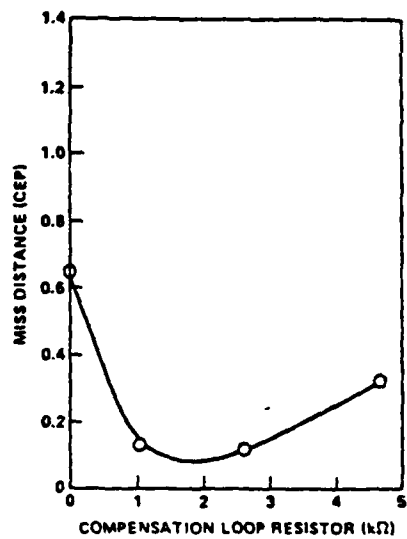


Fig. 16 Miss distance as a function of optical-gimbal coupling compensation.

Optical-gimbal coupling, mentioned previously, was found as a nonlinearity introduced into the seeker detector when the gimbal displacement permitted the laser beam to be received through the fixed lens on an axis offset from the center. An empirical correction was required for this in the form of a compensation loop in the gimbal torquer. Fig. 16 shows the variation of miss distance with a resistance value which determined the loop gain.

A total of over 1500 simulated flights were made on the two CLGP designs over a period extending from May 1973 to 1977. These include a sample of 11 projectiles by Martin-Marietta and 9 by Texas Instruments. Many variations were made on the simulation runs as described previously. Thus, it is difficult to categorize the data on an equal basis; however, certain statistics have been calculated and several examples are summarized here.

A total of 213 simulated flights was made on four Martin-Marietta CLGP rounds designed for firings at 8-km targets at WSMR. A total of 217 simulated flights was made on one Texas Instruments CLGP at various target ranges which eventually was air released at Edwards Air Force Base. A summary of these results is shown in Table 1 (normalized by circular error probability).

Table 1
SUMMARY OF CLGP SIMULATED FLIGHTS

<u>System</u>	<u>No. of Flights</u>	<u>Mean</u>	<u>Standard Deviation</u>
Texas Instruments: THU	91 at 4 km	2.41	2.32
	72 at 8 km	1.82	2.19
	54 at 12 km	0.76	0.68
	Total	217	1.81
Martin-Marietta: CG-1	36 at 8 km	1.34	0.69
	CG-2	53 at 8 km	1.36
	CG-3	76 at 8 km	1.12
	CG-4	48 at 8 km	2.4
Total	213	1.6 ^c	1.57

A summary of all simulated flights is given in Table 2 (normalized by circular error probability).

Table 2
HWIL SIMULATION RESULTS

<u>System</u>	<u>No. of Flights</u>	<u>Mean</u>	<u>Standard Deviation</u>
Texas Instruments	650	2.95	2.64
Martin-Marietta	808	1.72	1.47

Engineering Development Flight Test Results

The first flight demonstrations in engineering development (ED) took place in November 1976 to evaluate roll control and roll loop stability limitations. Fully guided ED flights were initiated in March 1977, and a total of 129 rounds had been flown as of August 1979. Hardware failures and incorrectly assumed aerodynamic characteristics prevented a successful demonstration until the fifth flight. Subsequently the high-g

capability of the components was proven. After successfully hitting a 7.7-km tank target, a series of successes followed at 16, 12, 11, 7.7, 5.6, 4, and 3 km range. The accuracy of the system (Fig. 17) has exceeded the requirement and all aspects of the guidance and control loop appear exceptional. Eighty-six rounds have achieved direct hits on targets. Targets have been accurately hit while moving at speeds up to 20 mph in both crossing and head-on attitudes. Compatibility with three different types of ground designators was demonstrated.

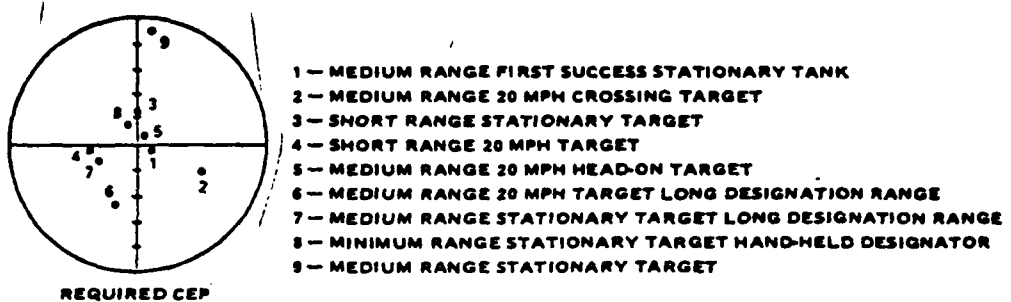


Fig. 17 Typical COPPERHEAD guidance and control performance.

VINDICATION BY FLIGHT

Two CLGP AD projectiles dedicated to the RPV designation demonstration⁶ were CG-11 and CG-12. The guidance sections from both units were evaluated in the HWIL simulation at the MICOM G&C analysis facility during July and August 1975. CG-12 operation was verified without incident, but three evaluations at MICOM were necessary before satisfactory performance was obtained with CG-11. The problem encountered at MICOM was an oscillation in the line-of-sight errors while in the high gain nulling mode. This prevented the unit from initiating guidance. The oscillation appeared only in a small region under certain gimbal angle ranges and gyro slew rates. This type problem had not been encountered on any previous units during AD. Attempts to diagnose the specific cause of the difficulty were unsuccessful; however, the condition was rectified by a gain reduction in the torquer loop and adjustment of the optical transfer functions by changing the gyro mirror position.

The seeker gyro for CG-11 was previously flown in a MICOM canister that experienced failure of the soft recovery system and was subjected to a hard impact. The seeker gyro was subsequently rebuilt from parts available inhouse. The electronic housing for CG-11 was previously discarded during fabrication due to cracked lands on the motherboard. The CG-11 guidance unit experienced another anomaly after it was hardened. The flight sequence logic used to delay seeker gyro track and start of guidance ceased to function. Interchanging of suspect components was unsuccessful and it was necessary to add a circuit modification to achieve satisfactory performance. After these problems were corrected, both units were integrated into all up rounds and subjected to limited environmental tests and inhouse acceptance tests. Both units were shipped to WSMR on 23 September 1975.

The RPV test contingent arrived at WSMR and eight dry run attempts were made between 24 and 28 September 1975 without satisfactory results. Problems were repeatedly encountered with the VEGA system and were solved only after replacement of the RPV transponders, repositioning of ground antennas and recalibration of the equipment. Difficulties were also encountered in trimming the autopilot and one engine failure occurred on takeoff. Though lasing was accomplished on a couple of passes, designation performance and RPV flight profile control were unacceptable.

In order to give increased realism to the joint demonstration, the decision was made to switch from a proposed 12 x 12 ft square white target panel to an M48 tank hulk. Reflectivity augmentation was approved and the target tank was taped with green missile tape. This produced a reflectivity of 15% (compared to the normal 5 to 10%) which provided adequate reflected energy for acquisition by CLGP.

On 29 September, during the 9th dry run, adequate flight profile control was demonstrated and seven lasing passes were made against the tank target. Designation tracking was good except for two problems. The tracking sight would periodically jump (as much as a degree) and the interface between the side and bottom of the optical dome would pass through the laser beam due to roll motion of the RPV. The sight jump was demonstrated to be caused by interference between VEGA and FPS-16 radars which were skin tracking the RPV. The RPV pilot was not aware of the scattering effects produced by the dome edge passing through the laser beam and he was instructed to maintain the roll attitude during the last 20 seconds of flight. The jump problem was solved by securing approval to drop radar track on the RPV (required by WSMR range safety) during the lasing leg of the racetrack. Though an additional dry run appeared desirable, the decision was made to attempt a firing on 3 October provided the above fixes could be demonstrated in preliminary passes against the target. This approach minimized the risks placed on the RPV by an additional takeoff and landing required by a dry run flight.

After the decision was made to proceed with the RPV demonstration, MGP-11 (CG-12) was hardened for flight. Final assembly and preparation included the epoxy hardening of the aft connector between the control and telemetry sections, final mating of control section to the telemetry section, and installation of the aft closure and obturator. During final assembly of MGP-11, the epoxy used to harden the connector did not set up properly and it was necessary to disassemble the round to reharden the connector. During disassembly, several of the control section connector wires were broken and could not be repaired in the field. It was necessary to replace the CG-12 control section with the section from CG-11, and repeat the projectile Acceptance Test Procedure.

On 3 October 1975, the RPV took off at 11:58 a.m. and made a total of nine passes against the target. The periodic jumps observed in the tracking sight were eliminated by shutting down the missile and RPV tracking radars but flight control adequate to proceed with a hot pass was not obtained. The RPV was landed at 14:27, refueled, and the VEGA transponder was replaced. The second takeoff occurred at 15:29, and

the RPV made five passes. Designation and tracking on the two lasing runs made prior to the hot pass were acceptable, flight profile control was much improved, and no tracking anomalies were encountered with both tracking radars shut off. The decision was then made to go for a hot pass.

CLGP was subsequently launched from the M109A1 at 1730 MDT on 3 October and approximately 30 seconds later it achieved a direct hit on the tank being designated by the RPV. Telemetry data did not reveal any projectile flight anomalies. Examination of the laser and designator video recordings did show that designation on the hot pass was not as stable as the two preceding dry run passes. However, after CLGP acquired at 15 seconds into the flight, it detected all pulses except for three instances, before impact. CLGP hit on top of the turret near the base of the gun tube and was pulling down at impact, which would produce a high obliquity angle at impact. At this angle and location, a high probability of kill would have been obtained. Fig. 18 shows the RPV and CLGP profile position during the actual flight test.

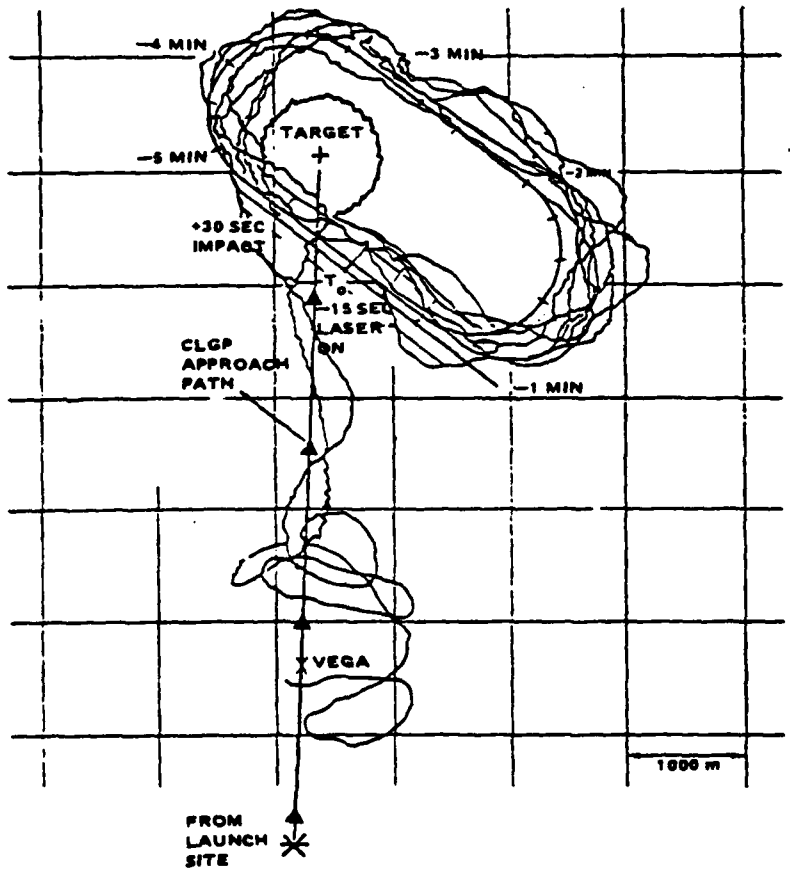


Fig. 18 RPV racetrack and profile position on launch flight.

CONCLUSIONS

A comprehensive HWIL simulation was developed to perform design verification and extensive statistical, stability, and miss distance performance analysis not available from an all-digital simulation. The results to date are indicative of the performance expected from CLGP.

The hybrid simulation development is time consuming and costly; however, it is an immensely powerful evaluation and synthesis tool. In addition to providing insight into the weapon system, it provides a real-world method for optimizing guidance parameters virtually on line. It represents the highest leveling dynamic validation programmable for a system short of performing an actual flight test.

REFERENCES

1. D. W. Sutherlin and K. V. Grider, "MICON's Advanced Simulation Center," Proceedings Symposium on Systems Theory, Auburn, Alabama, March 1975.
2. H. L. Pastrick, "Testing the Army's CLGP via Hardware-in-the-Loop Simulation," Proceedings Seventh National Guidance Test Symposium, Holloman Air Force Base, New Mexico, May 1975.
3. H. L. Pastrick, C. M. Will, L. S. Isom, L. H. Hazel, and R. J. Vinson, "Hardware-in-the-Loop Simulations: A Guidance System Optimization Tool," Paper 74-929, AIAA Mechanics and Control of Flight Conference, Anaheim, California, August 1974.
4. P. H. Morrison, "A Lesson Learned About Cannon-Launched Guided Projectiles," Paper 78-1244, AIAA Guidance and Control Conference, Palo Alto, California, August 1978.
5. R. J. Feist, "Opportunities for Cost Reductions in the Testing of New Missile Systems," US Army War College Essay, Carlisle Barracks, Pennsylvania, November 1975.
6. R. A. Nulk and H. L. Pastrick, "Flight Results and Analysis on Accurate Munitions Delivery Using CLGP with an RPV," Proceedings NATO/AGARD Conference on Avionics, Guidance and Control for RPVs, Italian Air War College, Florence, Italy, October 1976.

REFERENCES

¹Seltzer, S.M., "SAM: An Alternative to Sampled-Data Signal Flow Graphs," Technical Report T-79-49, US Army Missile Research and Development Command, May 1979.

²Seltzer, S.M., "Application of the Parameter Space Method to Aerospace Vehicle Digital Control System Design," IEEE Transactions on Automatic Control, Vol. AC-26, No. 2, April 1980, pp. 530-534.

³Seltzer, S.M., "Determination of Digital Control System Response by Cross-Multiplication," Technical Report T-79-58, US Army Missile Command, 29 May 1979.

DISTRIBUTION LIST

✓ Commander
Defense Documentation Center
ATTN: DDC-TCA
Cameron Station, Bldg. 5
Alexandria, VA 22314

DCASMA, Birmingham
908 South 20th Street
Birmingham, AL 35205

Commander
US Army Missile Command
Redstone Arsenal, AL 35898

ATTN: DRSMI-IYB/Glass

ATTN: DRSMI-IYB/Henderson

ATTN: DRSMI-RG

ATTN: DRSMI-RGN/McLean (3 copies)

DAT
FILM